Sorting of secretory proteins at the trans-Golgi network by TGN46

Pablo Lujan[1], Carla Garcia-Cabau[2,#], Yuichi Wakana[3,#], Javier Vera Lillo[1], Carmen Rodilla-Ramírez[1], Vivek Malhotra[4,5,6], Xavier Salvatella[2,6], Maria F. Garcia-Parajo[1,6], and Felix Campelo[1,*]

[1] ICFO-Institut de Ciencies Fotoniques, The Barcelona Institute of Science and Technology, 08860, Castelldefels (Barcelona), Spain.

[2] Institute for Research in Biomedicine (IRB Barcelona), The Barcelona Institute of Science and Technology, Baldiri Reixac 10, 08028, Barcelona, Spain.

[3] School of Life Sciences, Tokyo University of Pharmacy and Life Sciences, Hachioji, Tokyo 192-0392, Japan.

[4] Centre for Genomic Regulation (CRG), The Barcelona Institute of Science and Technology, Barcelona, Spain.

[5] Universitat Pompeu Fabra (UPF), Barcelona, Spain.

[6] Institució Catalana de Recerca i Estudis Avançats (ICREA), Passeig Lluís Companys 23, 08010, Barcelona, Spain.

[#] These authors contributed equally

[*] **Correspondence:**

Felix Campelo

ICFO-Institut de Ciencies Fotòniques

Av. Carl Friedrich Gauss, 3. 08860 Castelldefels, Barcelona - SPAIN

Phone: + 34 93 554 2225

e-mail: felix.campelo@icfo.eu

ABSTRACT

Secretory proteins are sorted at the trans-Golgi network (TGN) for export into specific transport carriers. However, the molecular players involved in this fundamental process remain largely elusive. Here, we identified the transmembrane protein TGN46 as a receptor for the export of secretory cargo protein PAUF in CARTS – a class of protein kinase D-dependent TGN-to-plasma membrane carriers. We show that TGN46 is necessary for cargo sorting and loading into nascent carriers at the TGN. By combining quantitative fluorescence microscopy and mutagenesis approaches, we further discovered that the lumenal domain of TGN46 encodes for its cargo sorting function. In summary, our results define a cellular function of TGN46 in sorting secretory proteins for export from the TGN.

KEYWORDS: Golgi apparatus, transport carrier, protein kinase D, export kinetics, membrane trafficking.

42 **INTRODUCTION**

43 Secretory proteins synthesized into the lumen of the ER are transported to the Golgi apparatus,
44 where they are further processed and eventually sorted at the *trans*-Golgi network (TGN) for
45 delivery to their respective destinations (Stalder and Gershlick, 2020; Wakana and Campelo,
46 2021; Spang, 2015; von Blume and Hausser, 2019; Di Martino et al., 2019). The accurate and
47 timely export of cargo proteins – such as collagens, hormones or neurotransmitters – is essential
48 for the maintenance of cell and tissue homeostasis. Accordingly, errors in this process can have
49 severe physiological and pathophysiological consequences (Zappa et al., 2018). Despite the
50 importance of this process, the molecular machinery and the mechanisms of cargo sorting at
51 the TGN remain largely elusive (Guo et al., 2014; Boncompain and Weigel, 2018; Ford et al.,
52 2021; Ramazanov et al., 2021). In mammalian cells, lysosomal hydrolases bearing a mannose
53 6-phosphate are sorted by the mannose 6-phosphate receptors into clathrin-coated vesicles for
54 their transport to the endo-lysosomal system (Kienzle and von Blume, 2014; Braulke and
55 Bonifacino, 2009). By contrast, no protein coats have been identified for most export routes
56 from the TGN – especially for those destined to the cell surface (Stalder and Gershlick, 2020;
57 Wakana and Campelo, 2021) –, which has hampered the identification of cargo receptors or of
58 other sorting modules. The discovery by Malhotra and colleagues of a Ca^{2+}-dependent
59 mechanism for the sorting of a subset of soluble secretory cargoes is beginning to reveal the
60 intricacies of this supposedly receptor-independent process (von Blume et al., 2009; Curwin et
61 al., 2012). This mechanism relies on the coordinated action of various cellular components,
62 including the actin filament-severing protein cofilin (von Blume et al., 2009; Curwin et al.,
63 2012), the Ca^{2+} pump SPCA1 (von Blume et al., 2011; Kienzle et al., 2014), the oligomeric
64 lumenal Ca^{2+}-binding protein Cab45 (Crevenna et al., 2016; von Blume et al., 2012), and the
65 sphingolipid sphingomyelin (SM) (Deng et al., 2016, 2018). The export from the Golgi by this
66 pathway is independent of any coat proteins identified thus far. However, how other soluble
67 cargo proteins are sorted for their export from the TGN remains unknown.

68 The single-pass type I transmembrane (TM) protein TGN46 – or TGN38 in rodents
69 (Ponnambalam et al., 1996) – has been proposed to function as a secretory cargo receptor
70 (Stanley and Howell, 1993; Jones et al., 1993; Wang et al., 1995; Banting and Ponnambalam,
71 1997; McNamara et al., 2004; Wang and Howell, 2000; Ramazanov et al., 2021). However,
72 direct evidence for a role of TGN46 in Golgi export is lacking. TGN38 was first identified in
73 rat cells and shown to have a well-defined steady-state localization at the TGN (Luzio et al.,
74 1990). As a result, TGN38 and its orthologues have become extensively employed as TGN
75 marker proteins. Remarkably, the amino acid sequence of rat TGN38 is largely conserved
76 amongst other species, including humans (>80% amino acid identity between rat TGN38 and
77 human TGN46), with highly-conserved cytosolic and TM domains and a somewhat less

78 conserved lumenal domain (>60% overall identity but only ~25% in the bulk of the lumenal
79 domain) (Ponnambalam et al., 1996). Despite having a steady-state TGN localization,
80 TGN38/TGN46 rapidly cycles between the TGN and the plasma membrane (PM), exiting the
81 TGN in specific carriers called CARTS (carriers of the TGN to the cell surface) (Wakana et al.,
82 2012) and recycling from the PM back to the Golgi via early endosomes (Banting and
83 Ponnambalam, 1997; Bos et al., 1993; Rajasekaran et al., 1994; Mallet and Maxfield, 1999;
84 Humphrey et al., 1993). CARTS were first identified by immuno-isolation of TGN46-
85 containing transport carriers from the TGN to the PM (Wakana et al., 2012). CARTS are formed
86 in a protein kinase D (PKD)-dependent manner and contain the Rab6/Rab8 GTPases. CARTS
87 traffic specific secretory cargoes, such as pancreatic adenocarcinoma upregulated factor
88 (PAUF) and LyzC , while exclude others, such as collagen I or VSVG (Wakana et al., 2012,
89 2013; Wakana and Campelo, 2021; Lujan et al., 2021). However, how secretory cargoes are
90 sorted and specifically packed into CARTS is yet to be understood. Furthermore, whether
91 TGN46 plays an active role in CARTS biogenesis or it is just a passive transmembrane cargo
92 of this pathway is still unknown.

93 Here, we demonstrate that TGN46 plays a key role in constitutive protein secretion, specifically
94 in the sorting of the soluble cargo protein PAUF into CARTS for TGN export. Our data reveal
95 that the topological determinants that describe the proper intracellular and intra-Golgi
96 localization of TGN46, as well as its own incorporation in CARTS, are mainly contained in its
97 lumenal domain. Notably, we find that the lumenal domain of TGN46 is both necessary and
98 sufficient for the export of cargo proteins into CARTS and, moreover, that this domain mediates
99 the cargo sorting function of TGN46. Altogether, our data suggest an essential role for TGN46
100 in the sorting of cargo proteins into transport carriers (CARTS) at the TGN.

101

102 **RESULTS**

103 **TGN46 is required for cargo sorting into CARTS**

104 As TGN46 has been suggested, but not shown, to function in cargo sorting at the TGN, we
105 decided to test this hypothesis. We generated a TGN46-lacking line of Hela cells by
106 CRISPR/Cas9-mediated knock out of *TGOLN2* – the gene encoding for human TGN46
107 (TGN46-KO cell line) (***Fig. 1A*** and ***Fig. S1A***). To test if TGN46 is required for CARTS-
108 mediated secretion, we transiently expressed a CARTS-specific soluble cargo protein, PAUF-
109 MycHis, in both parental and TGN46-KO cells. Both the medium and cell lysates were
110 collected and analyzed by western blotting with an anti-Myc antibody to detect the secreted and
111 internal PAUF-MycHis pools, respectively. In TGN46-KO cells, PAUF-MycHis secretion was
112 reduced by ~75% as compared to control cells (***Fig. 1A***). We noticed the appearance of a lower

113 molecular weight form of PAUF-MycHis in the lysate of TGN46-KO cells (***Fig. 1A***),
114 suggesting that the processing (e.g., glycosylation) of intracellularly accumulated PAUF-
115 MycHis is incomplete, and opening the possibility of a role for TGN46 in facilitating cargo
116 glycosylation. Immunofluorescence microscopy of cells expressing PAUF-mRFP revealed its
117 presence in a perinuclear compartment in both parental and TGN46-KO cell lines, indicating
118 that PAUF-mRFP efficiently exits the ER in the absence of TGN46 (***Fig. S1A***).

119 To test whether TGN46 is specifically involved in the secretion of CARTS-mediated cargoes
120 or rather plays a general role in TGN export, we simultaneously monitored Golgi export of
121 PAUF-mRFP (a CARTS cargo) and VSVG-HA (a non-CARTS cargo) (Wakana et al., 2012;
122 Wakana and Campelo, 2021) in parental and TGN46-KO cells. We used the standard
123 temperature-induced block in cargo export at the TGN to monitor synchronous exit of VSV-G
124 or PAUF in control and TGN46-lacking cells. Cells were first incubated at 20ºC for 2h to block
125 TGN export, and subsequently shifted to 37ºC for 15 min to allow for synchronized export from
126 the TGN, after which cells were fixed and the number of cargo-containing vesicular structures
127 per unit area was analyzed by confocal fluorescence microscopy (***Fig. 1B*** and ***Fig. S1B***). Our
128 data show that the number density of PAUF-mRFP-positive punctate structures – which define
129 CARTS (Wakana et al., 2012) – is significantly reduced by ~50% in TGN46-KO cells as
130 compared to parental cells (***Fig. 1B***). These results agree with and complement the observed
131 inhibition of PAUF secretion in the absence of TGN46 (***Fig. 1A***). By contrast, the number
132 density of VSVG-containing carriers was unaltered upon TGN46 depletion (***Fig. 1B*** and ***Fig.***
133 ***S1B***), indicating that TGN46 selectively functions in the export of a subset of cargo proteins at
134 the TGN. In addition, TGN46 depletion did not increase the proportion of CARTS (defined as
135 carriers positive for PAUF) that also contained VSVG (***Fig. S1C***). These data strongly suggest
136 that, in the absence of TGN46, PAUF is not re-routed towards alternative TGN export routes
137 (particularly to that of VSV-G-containing transport carriers), and therefore bona fide CARTS
138 are still formed, although at a strongly reduced rate. Hence, we will use PAUF as a marker
139 protein for CARTS throughout this article.

140 We next assessed by fluorescence loss in photobleaching (FLIP) microscopy the residence time
141 of PAUF in the Golgi apparatus, which is a dynamic measure of the Golgi export rate of this
142 cargo (***Fig. S1D***) (Hirschberg et al., 1998; Patterson et al., 2008). In our FLIP experiments, we
143 systematically photobleached by using a high intensity laser the entire pool of fluorescent
144 protein (e.g., PAUF-mRFP) located outside of the perinuclear Golgi area, and measured the
145 decay of the fluorescence intensity of the Golgi area as function of time (***Fig. S1D***). Thus, for
146 cargo proteins that are rapidly exported from the Golgi, the fluorescence intensity in the Golgi
147 area is expected to rapidly decay, whereas for resident Golgi proteins, the fluorescence should
148 decay more slowly. Our results showed that PAUF-mRFP has a longer Golgi residence time in

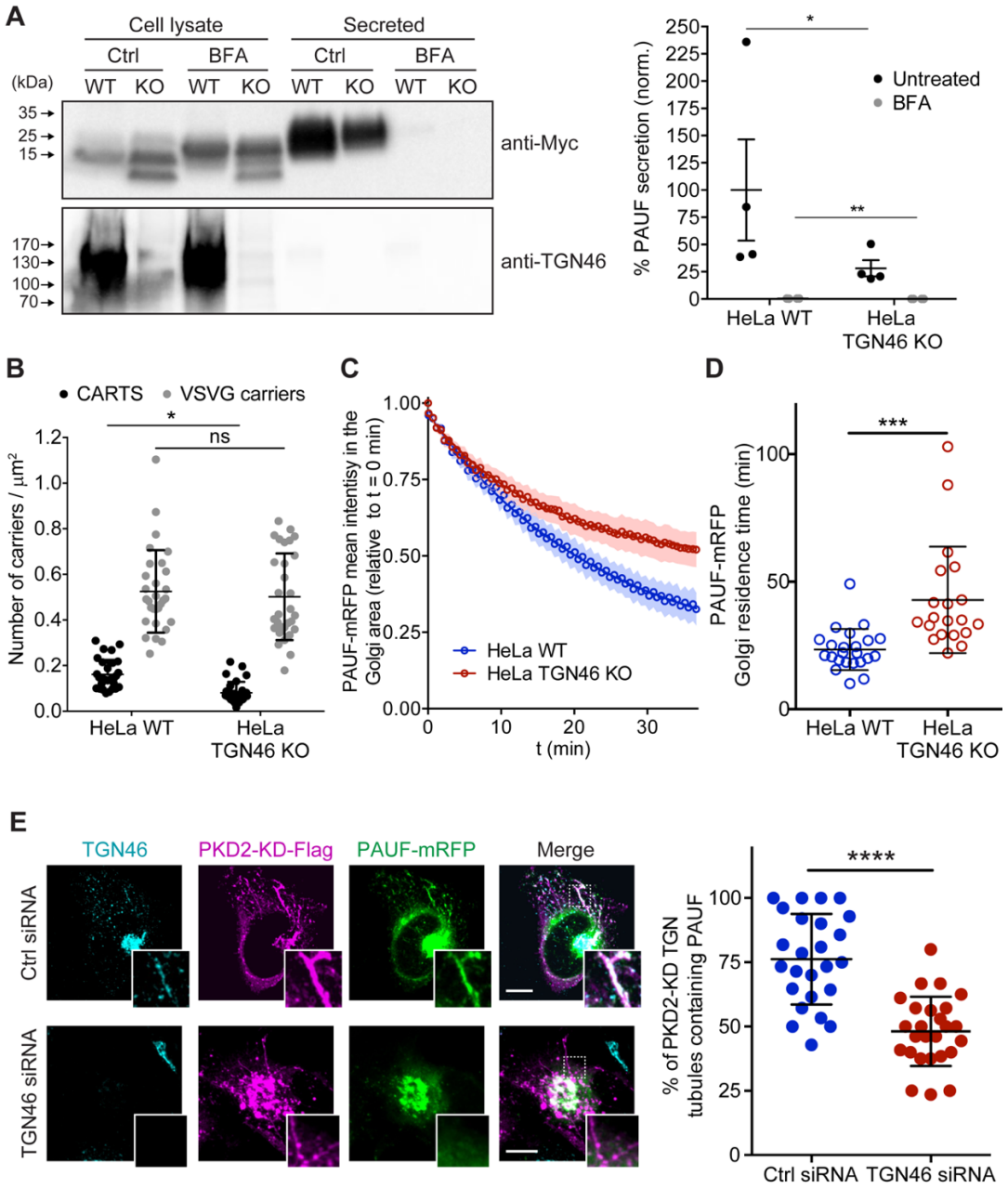

Figure 1. TGN46 is required for cargo sorting and loading into CARTS. (A) PAUF secretion assay in parental (WT) and CRISPR/Cas9-mediated TGN46 knockout (KO) HeLa cells. Cells expressing PAUF-MycHis were incubated for 4 h in fresh medium without serum in the absence (Ctrl) or presence of Brefeldin A (BFA), after which the cells were lysed. Equal amounts of cell lysates and their corresponding secreted fraction (medium) were analyzed by western blotting (left) using an anti-Myc antibody (top blot) and anti-TGN46 antibody (bottom blot). BFA was included as a positive control of secretion inhibition. Quantification (right) of the ratio of secreted/internal PAUF signal normalized (norm.) as a percentage to the average value of the WT, Ctrl condition. n=4 independent experiments. Individual values shown, with mean ± stdev. **(B)** Number of carriers (CARTS, black symbols; VSVG carriers, gray symbols) per unit area observed in WT or TGN46-KO HeLa cells expressing either PAUF-mRFP (CARTS marker) and VSVG-HA (VSVG carrier marker). At least 10 cells from each of n=3 independent experiments were quantified. Individual values shown, with mean ± stdev. **(C)** Relative fluorescence intensity average time trace (mean ± s.e.m.) of FLIP experiments performed in WT or TGN46-KO HeLa cells expressing PAUF-mRFP. **(D)** Quantification of the PAUF-mRFP Golgi residence time as obtained from the FLIP experiments, as the one shown in **(C)**. Between 7–12 cells from each of n=3 independent experiments were quantified. Individual values shown, with mean ± stdev. **(E)** Left panels are confocal fluorescence microscopy images of HeLa cells transfected with control (Ctrl) or TGN46 siRNA, which were also transfected with PKD2-KD-Flag and PAUF-mRFP. Cells were fixed at steady state and labelled with anti-TGN46 (cyan) and anti-Flag (magenta) antibodies. PAUF-mRFP fluorescence signal is shown in green. Scale bars are 10 µm, magnifications of the boxed regions are shown. In the right panel, the quantification of the percentage of PKD2-KD-induced tubules that containg PAUF-mRFP in control (Ctrl) or TGN46 siRNA-treated cells. At least 10 cells from each of n=3 independent experiments. Individual values shown, with mean ± stdev.

149 TGN46-KO cells (~40 min) as compared to control cells (~25 min), and therefore TGN46 is
150 necessary for an efficient and fast export of PAUF (***Fig. 1C,D*** and ***Fig. S1D***). Taken together,
151 our results indicate that TGN46 is necessary for CARTS-mediated PAUF export from the TGN.

152 **TGN46 is required for cargo loading into CARTS**

153 Cargo-loaded CARTS detach from the TGN once the neck of the nascent carrier is severed
154 through a membrane fission reaction, a process regulated by the kinase activity of PKD
155 (Wakana et al., 2012). Accordingly, expression of a kinase-dead mutant of PKD (PKD-KD)
156 leads to the formation of cargo-loaded tubules (fission-defective CARTS precursors) at the
157 TGN (Malhotra and Campelo, 2011; Wakana and Campelo, 2021). We took advantage of this
158 to test if TGN46 is needed for cargo loading into CARTS and/or for membrane bending. We
159 co-transfected PAUF-mRFP and PKD2-KD-Flag in control and TGN46-depleted HeLa cells,
160 after which cells were fixed and processed for immunofluorescence microscopy. We first
161 observed that TGN46 depletion did not affect the number or appearance of PKD2-KD-positive
162 TGN tubules per cell (***Fig. 1E*** and ***Fig. S1E***), suggesting that TGN46 is not necessary for
163 membrane bending. Next, we observed that in control (TGN46-positive) cells, a large fraction
164 of Golgi tubules contained both TGN46 and PAUF-mRFP (~75±15% of tubules containing
165 PAUF) (***Fig. 1E***), as previously described (Liljedahl et al., 2001; Wakana et al., 2012). In
166 contrast, and remarkably, PAUF-mRFP was absent from the majority of the tubules induced by
167 PKD-KD in TGN46-depleted cells (~45±10% of tubules containing PAUF) (***Fig. 1E*** and ***Fig.***
168 ***S1E***). These findings strongly indicate that TGN46 is required for sorting and loading the
169 secretory cargo protein PAUF into nascent CARTS at the TGN.

170 **TGN46 export in CARTS is not dependent on TGN46 cytosolic tail signals**

171 Although a number of sequence motifs have been reported to serve as retention signals for
172 Golgi-resident proteins (Welch and Munro, 2019; Lujan and Campelo, 2021), less is known
173 about how cargoes are selectively sorted into transport carriers budding from the TGN.
174 Particularly, sorting mechanisms for CARTS-specific cargoes remain elusive (Wakana and
175 Campelo, 2021). To investigate how TGN46 sorts cargoes into CARTS, we employed a
176 mutagenesis approach to examine whether TGN46 possesses specific topological determinants
177 (such as domains, regions, or motifs) responsible for its cargo sorting and packaging function.
178 As TGN46 is a single-pass type I TM protein of 437 amino acids (human TGN46, UniProt
179 identifier O43493-2), we investigated whether functional cargo-packaging modules can be
180 found in *(i)* the N-terminal lumenal domain (amino acids 22–381), *(ii)* the single TM domain
181 (TMD; amino acids 382–402), and/or *(iii)* the short C-terminal cytosolic tail (amino acids 403–
182 437). In particular, we generated a battery of mutant proteins and evaluated how they behave

183 in terms of *(i)* their fine intra-TGN protein localization, *(ii)* their specific sorting into CARTS,
184 and *(iii)* their Golgi export rate.

185 We start by investigating the existence of sorting signals in the cytosolic tail of TGN46. This
186 tail region contains a tyrosine-based cytosolic motif (YXXΦ; where X represents any amino
187 acid, and Φ is an amino acid with bulky hydrophobic side chains (Ohno et al., 1996); in TGN46:
188 YQRL, amino acids 430-433). This motif acts as an endocytic signal for PM internalization
189 and trafficking back to the TGN, and is therefore crucial for the steady-state localization of
190 TGN46 at TGN (Banting and Ponnambalam, 1997; Stanley and Howell, 1993; Rajasekaran et
191 al., 1994; Bos et al., 1993; Humphrey et al., 1993; Banting et al., 1998). We expressed in HeLa
192 cells a GFP-tagged deletion mutant of TGN46 lacking the cytosolic domain but maintaining
193 the lumenal domain and TMD (GFP-TGN46-Δcyt) (***Fig. 2A***) and analyzed its intracellular
194 localization by fluorescence microscopy. As previously reported (Bos et al., 1993; Humphrey
195 et al., 1993), GFP-TGN46-Δcyt was partially present at the *trans*-Golgi membranes/TGN and
196 partially at the plasma membrane, as qualitatively seen in the micrographs (***Fig. S2***). We and
197 others have previously shown that the *trans*-Golgi/TGN membranes are laterally
198 compartmentalized into export domains (positive for TGN46) and processing domains (positive
199 for the late-Golgi glycosylation enzyme sialyltransferase, ST) (van Galen et al., 2014; Patterson
200 et al., 2008; Tie et al., 2022). We therefore quantitatively measured whether GFP-TGN46-Δcyt
201 partitions into export or processing subdomains. To that end, we co-expressed either GFP-
202 TGN46 WT or GFP-TGN46-Δcyt together with TGN46-mRFP or ST-mCherry, and measured
203 the degree of perinuclear colocalization between the different protein pairs (Pearson's
204 correlation coefficient (Dunn et al., 2011)) (***Fig. 2B*** and ***Fig. S2A***). Our data show that GFP-
205 TGN46-Δcyt has a lower degree of intra-Golgi colocalization with respect to TGN46-mRFP
206 and a higher one with respect to ST-mCherry, as compared to its WT counterpart (***Fig. 2B*** and
207 ***Fig. S2A***). Hence, GFP-TGN46-Δcyt shows an intra-Golgi localization pattern more closely
208 resembling that of ST-GFP-positive processing domains (***Fig. 2B*** and ***Fig. S2A***). These data
209 indicate that the cytosolic domain of TGN46 confers an overall TGN localization by
210 contributing not only to the recycling from the PM, as previously reported (Bos et al., 1993;
211 Humphrey et al., 1993), but also to its fine steady-state partitioning into TGN export domains
212 and exclusion from processing domains. We next tested how GFP-TGN46-Δcyt is exported
213 from the TGN. We first monitored the incorporation of GFP-TGN46-Δcyt into CARTS. HeLa
214 cells co-overexpressing GFP-TGN46-Δcyt together with either PAUF-mRFP (CARTS marker)
215 or VSVG-HA (a CARTS-independent TM cargo protein) were incubated at 20ºC for 2 h to
216 inhibit TGN export, shifted to 37ºC for 15 min to re-initiate cargo export, fixed, and imaged by
217 fluorescence microscopy. We then analyzed the fraction of cargo-containing carriers (for three
218 different cargoes: GFP-TGN46 WT, VSVG-HA, and GFP-TGN46-Δcyt) that were also

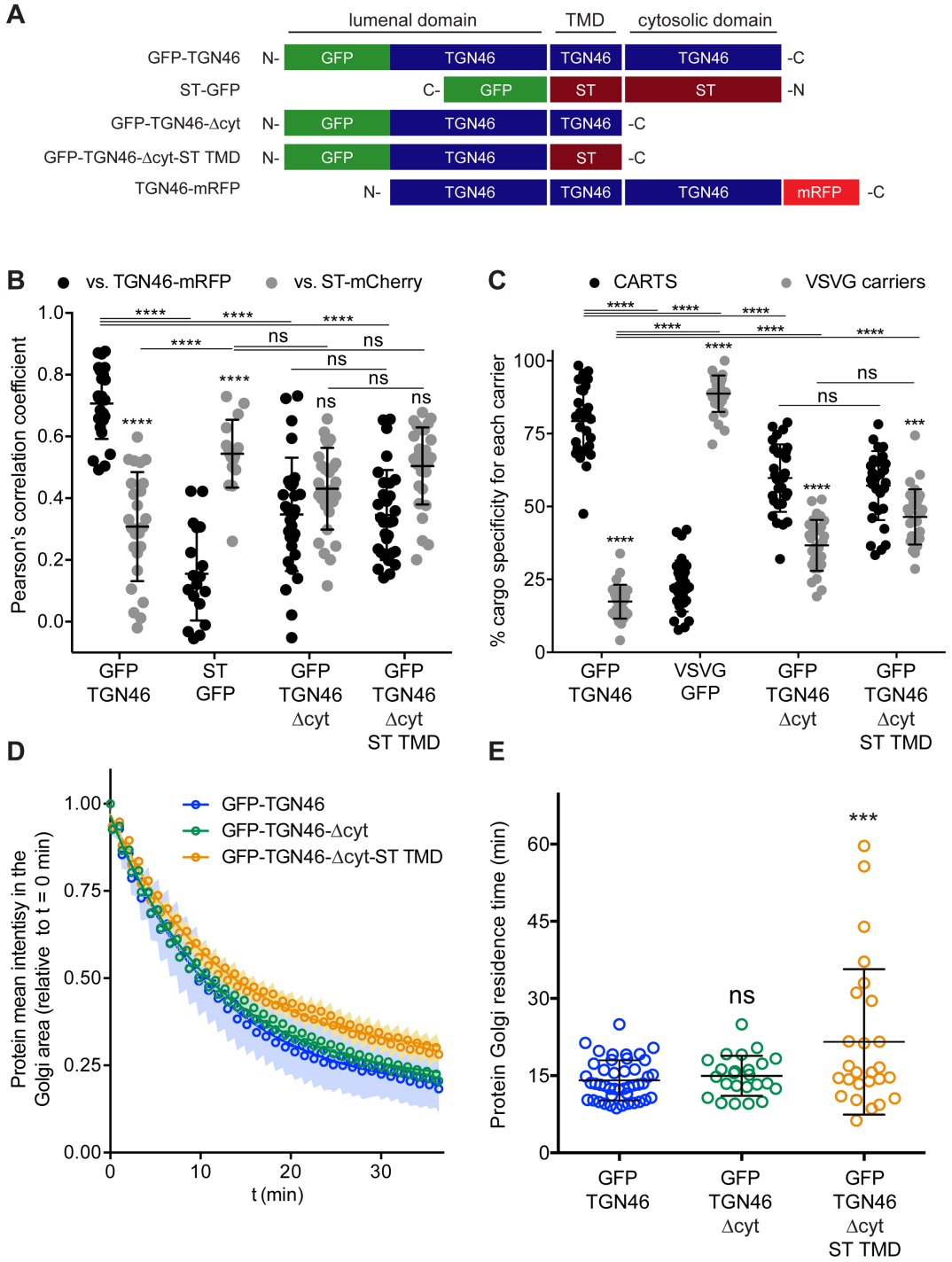

Figure 2. TGN46 export in CARTS is not dependent on cytosolic tail signals. (A) Schematic representation of construct domain topology. Notice that type I proteins (e.g., GFP-TGN46) have a lumenal N-terminal domain, whereas type II proteins (e.g., ST-GFP) have a cytosolic N-terminal domain. TMD: transmembrane domain. **(B)** Pearson's correlation coefficient between the perinuclear fluorescence signal of the x-axis indicated proteins with respect to TGN46-mRFP (black symbols) or ST-mCherry (gray symbols), measured from confocal micrographs of HeLa cells expressing the indicated proteins. Results are from at least 10 cells from each of n=3 independent experiments (individual values shown, with mean ± stdev). **(C)** Percentage of transport carriers containing each of the cargoes described on the x-axis that are also positive for PAUF (CARTS, black symbols) or VSVG (VSVG carriers, gray symbols), as measured from confocal micrographs of HeLa cells expressing the indicated proteins. Results are from at least 10 cells from each of n=3 independent experiments (individual values shown, with mean ± stdev). **(D)** Relative fluorescence intensity average time trace (mean ± s.e.m.) of FLIP experiments for the indicated proteins. Symbols correspond to actual measurements, solid lines to the fitted exponential decays. **(E)** Residence time in the perinuclear area measured as the half time of the FLIP curves. Results are from 7–12 cells from each of n=3 independent experiments (individual values shown, with mean ± stdev).

219 positive for PAUF-mRFP (CARTS) or VSVG-HA (VSVG carriers). Our results indicated that
220 GFP-TGN46-Δcyt is preferentially exported in CARTS and not in VSVG carriers, although
221 this mutant cargo protein showed a modest but statistically significant reduction in its CARTS
222 specificity as compared to GFP-TGN46 WT (***Fig. 2C*** and ***Fig. S2B***). We next performed FLIP
223 experiments to measure the Golgi residence time of GFP-TGN46-Δcyt, and compare it with
224 that of GFP-TGN46 WT. Interestingly, GFP-TGN46-Δcyt exits the Golgi at a rate that is
225 indistinguishable from that of GFP-TGN46 WT (***Fig. 2D,E*** and ***Fig. S2C***). Taken together, our
226 results suggest that, although the cytosolic tail of TGN46 is important for PM recycling, it does
227 not play a major role in mediating TGN46 incorporation into CARTS for export out of the
228 TGN.

229 **TGN46 intra-Golgi localization and CARTS specificity are insensitive to the length and**
230 **composition of its TMD**

231 We next investigated if the information encoded in the amino acid sequence of the TGN46
232 TMD determines its incorporation into CARTS. The hydrophobic matching hypothesis is a
233 TMD-based sorting mechanism that has been proposed to contribute to the retention of Golgi-
234 resident TM proteins (Welch and Munro, 2019; Lujan and Campelo, 2021). This mechanism is
235 based on the hypothesis that single-pass TM proteins preferably partition into membrane
236 regions of a thickness that best matches the hydrophobic length of the protein TMD (Munro,
237 1991; Sharpe et al., 2010; Munro, 1995). The membrane thickness increases along the secretory
238 pathway (Mitra et al., 2004), which correlates with the average TMD length of the proteins of
239 these organelles (Sharpe et al., 2010). Hence, according to the TMD-based retention hypothesis,
240 the separation between Golgi-resident proteins and cargoes destined for export from the TGN
241 is attributed to the distinct physical properties of these domains (Sharpe et al., 2010; Munro,
242 1995; Quiroga et al., 2013; Cosson et al., 2013). TGN46 is a type I protein with a single TMD
243 of 21 amino acids, whereas ST (ST6Gal-I) is a type II protein with a shorter TMD of 17 amino
244 acids (***Fig. 3A***). Thus, we generated two different TGN46 mutants by altering its TMD
245 sequence to test whether the length and/or amino acid composition of the TMD of TGN46 is
246 important for its characteristic intra-Golgi localization, selective CARTS-mediated export, and
247 Golgi residence time. The first mutant (TGN46-shortTMD) is a TGN46 deletion that lacks 4
248 amino acids (AAIL) in the central region of the TMD. For the second mutant (TGN46-ST
249 TMD), we replaced the TGN46 TMD by that of ST, while keeping the topology and, therefore,
250 the correct TMD orientation with respect to the bilayer (***Fig. 3A***). As compared to TGN46 WT,
251 both mutants have shorter TMDs (17 amino acids) and while TGN46-shortTMD maintains the
252 overall amino acid composition, TGN46-ST TMD has a completely altered TMD composition
253 (***Fig. 3A***).

254 First, we expressed different combinations of these proteins in HeLa cells, and monitored their
255 intracellular localization by fluorescence microscopy. Altering the TMD of TGN46 had no
256 discernible impact on intra-Golgi localization (***Fig. 3B*** and ***Fig. S3A***), suggesting that the
257 hydrophobic matching mechanism is not a major determinant for the fine intra-Golgi
258 localization of TGN46. Interestingly, even in cells treated with short-chain ceramide (D-
259 ceramide-C6), a treatment that causes morphological changes and the physical segregation of
260 the Golgi membranes into distinct ST- and TGN46-positive Golgi subdomains (Duran et al.,
261 2012; van Galen et al., 2014; Campelo et al., 2017; Capasso et al., 2017), we did not observe
262 any apparent change in the localization of the TGN46 mutants with short TMD with respect to
263 TGN46 WT (***Fig. S4***). However, because our results were obtained using diffraction-limited
264 confocal microscopy (with a spatial lateral resolution of ~250 nm), it is still possible that more
265 subtle alterations in the intra-Golgi localization of these mutants exist at shorter length scales.
266 To address this possibility, we used super-resolution single molecule localization microscopy
267 (SMLM) with a localization precision (resolution) of ~15–30 nm. Our results show that, even
268 with this enhanced spatial resolution, the intra-Golgi localization of the different TGN46
269 mutants with shorter TMD was indistinguishable from that of TGN46 WT (***Fig. S5***).

270 Second, we asked whether the TGN46 TMD sequence plays a role in dragging this protein into
271 CARTS. Interestingly, the two mutants with shorter TMDs (TGN46-shortTMD and TGN46-
272 ST TMD) lost their preference for being co-packaged with PAUF into CARTS, and partially
273 redirected into other transport carriers such as VSVG carriers (***Fig. 3C*** and ***Fig. S3B***).

274 Finally, we investigated how fast these TGN46 mutants with shorter TMDs are exported out of
275 the Golgi apparatus. FLIP experiments indicated that the chimeric protein TGN46-ST TMD-
276 GFP has a slower Golgi export rate (longer Golgi residence time) as compared to TGN46-GFP.
277 In addition, TGN46-shortTMD-GFP was exported at a slightly slower rate, although this
278 difference was not statistically significant (***Fig. 3D, E*** and ***Fig. S3C***). Next, we co-
279 overexpressed TGN46-GFP together with TGN46-ST TMD-mRFP or TGN46-mRFP, as a
280 control, and performed FLIP experiments tso measure the rate of TGN46 WT-GFP export. The
281 aim of these experiments was to test if the expression of these mutants leads to defects in
282 CARTS biogenesis. Our results show that the Golgi residence time of TGN46-GFP was not
283 affected by the co-expression of either the WT or the chimeric proteins (***Fig. S6A,B***). These
284 data provide further support to the idea that the slower Golgi export rate of TGN46 mutants
285 with short TMDs is a consequence of their compromised selective sorting into CARTS.

286 It has been reported that some medial Golgi enzymes can dimerize or oligomerize and that this
287 property (kin recognition) is important for TM protein localization along the Golgi stack
288 (Welch and Munro, 2019; Banfield, 2011; Lujan and Campelo, 2021). However, there are

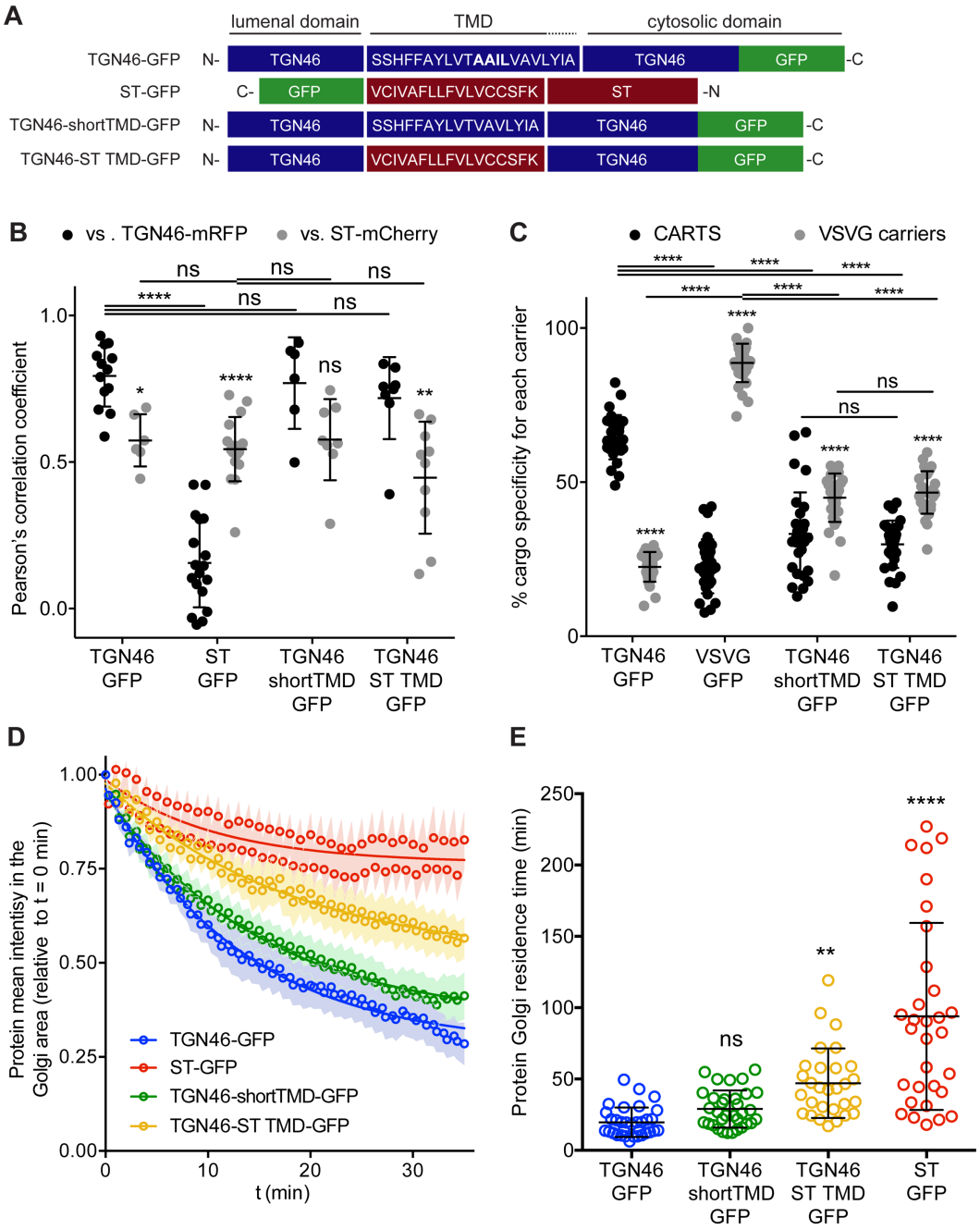

Figure 3. TGN46 intra-Golgi localization and CARTS specificity are insensitive to TMD length and composition. (A) Schematic representation of construct domain topology. The amino acid sequence (in the correct topology) of the different transmembrane domains (TMD) is indicated. **(B)** Pearson's correlation coefficient between the perinuclear fluorescence signal of the x-axis indicated proteins with respect to TGN46-mRFP (black symbols) or ST-mCherry (gray symbols), measured from confocal micrographs of HeLa cells expressing the indicated proteins. Results are at least 3 cells from each of n=3 independent experiments (individual values shown, with mean ± stdev). **(C)** Percentage of transport carriers containing each of the cargoes described on the x-axis that are also positive for PAUF (CARTS, black symbols) or VSVG (VSVG carriers, gray symbols), as measured from confocal micrographs of HeLa cells expressing the indicated proteins. Results are from at least 10 cells from each of n=3 independent experiments (individual values shown, with mean ± stdev). **(D)** Relative fluorescence intensity average time trace (mean ± s.e.m.) of FLIP experiments for the indicated proteins. Symbols correspond to actual measurements, solid lines to the fitted exponential decays. **(E)** Residence time in the perinuclear area measured as the half time of the FLIP curves. Results are from 7–12 cells from each of n=3 independent experiments (individual values shown, with mean ± stdev).

289 reports showing that kin recognition is not relevant for ST or for other *trans*-Golgi membrane
290 proteins (Munro, 1995). To examine if the unaltered intra-Golgi localization of TGN46-
291 shortTMD and TGN46-ST TMD compared to WT was due to protein
292 dimerization/oligomerization, we tested whether TGN46-GFP and TGN46-mRFP co-
293 immunoprecipitated when expressed in HeLa cells. Our results show no obvious dimerization
294 between TGN46-GFP and TGN46-mRFP (***Fig. S6C***).

295 One of the possible consequences of shortening the TMD of TGN46 might be the partial burial
296 of the highly charged residues of TGN46 cytosolic tail into the cytosolic leaflet of the TGN
297 membrane, which, concomitantly, could negatively hamper its CARTS-mediated export. If so,
298 the observed phenotype would follow from the unnatural proximity of the cytosolic tail to the
299 membrane rather than from a direct effect due to hydrophobic mismatch. To test this hypothesis,
300 we deleted the cytosolic tail of TGN46-ST TMD – which, as we showed earlier (***Fig. 2***), has
301 no major effect in TGN46 export in CARTS – to generate a mutant with TGN46 lumenal
302 domain, ST TMD, and no cytosolic tail (TGN46-Δcyt-ST TMD, ***Fig. 2A***). This chimeric
303 protein phenocopies GFP-TGN46-Δcyt regarding its *(i)* intra-Golgi localization (***Fig. 2B*** and
304 ***Fig. S2A***), and *(ii)* CARTS specificity (***Fig. 2C*** and ***Fig. S2B***), with only a milder reduction in
305 the Golgi export rate (***Fig. 2D,E*** and ***Fig. S2C***). Taken together, these results strongly indicate
306 that the hydrophobic matching mechanism (as well as the information encoded in the TMD)
307 does not play a primary role in driving the intra-Golgi localization and Golgi export of TGN46.

308 **The lumenal domain of TGN46 is necessary and sufficient for CARTS-mediated export**
309 **from the TGN**

310 Finally, we enquired if the lumenal domain of TGN46 plays a role in intra-Golgi localization,
311 Golgi export rate (residence time), and selective sorting into CARTS. First, we aimed to test
312 whether the lumenal domain of TGN46 is *necessary* for its sorting and packaging into CARTS.
313 We thus generated a deletion mutant of TGN46 lacking its lumenal domain (GFP-TGN46-
314 Δlum) (***Fig. 4A***), expressed it in parental HeLa cells, and monitored its intra-Golgi localization
315 by fluorescence microscopy. Although still perinuclear, GFP-TGN46-Δlum lost the
316 characteristic intra-Golgi localization of the TGN46 WT and rather localized into ST-mCherry-
317 positive processing domains of the *trans*-Golgi membranes (***Fig. 4B*** and ***Fig. S5A***). Notably,
318 this exclusion from TGN export domains paralleled a striking reduction in the selective
319 incorporation of GFP-TGN46-Δlum into CARTS (***Fig. 4D*** and ***Fig. S6A***), as well as in the rate
320 of Golgi export (***Fig. 4F*** and ***Fig. S7A,C***), as compared to the full length protein. These results
321 consistently indicate that the lumenal domain of TGN46 is *necessary* for CARTS-mediated
322 export of TGN46, therefore suggesting that this domain contains a signal for sorting and loading
323 into CARTS.

324 Next, we asked whether the TGN46 lumenal domain is not only necessary but also *sufficient*
325 for CARTS-mediated TGN exit. We started by generating a soluble cargo protein that only
326 contains the lumenal domain of TGN46, tagged with GFP at the N terminus just following the
327 signal sequence (GFP-TGN46lum) (***Fig. 4A***). Upon expression in HeLa cells, GFP-TGN46lum
328 localizes to the Golgi apparatus where it only shows a partial colocalization with TGN46-mRFP
329 or with ST-mCherry (***Fig. 4B*** and ***Fig. S7A***). This low degree of colocalization could be due to
330 the fact that we are comparing the location of soluble and TM proteins. Nonetheless, when we
331 used our synchronized cargo release assay to measure selective incorporation into CARTS,
332 GFP-TGN46lum maintained specificity for CARTS-mediated export (***Fig. 4D*** and ***Fig. S8A***).
333 Moreover, FLIP experiments revealed that GFP-TGN46lum exits as fast as GFP-TGN46 WT,
334 or even faster (***Fig. 4E*** and ***Fig. S9A,B***). We next asked if the signal encoded in the TGN46
335 lumenal domain can direct otherwise unrelated proteins into CARTS. In particular, we tested
336 whether TGN46 lumenal domain can lead to CARTS-mediated export of *(i)* a Golgi-resident
337 TM protein (ST), and *(ii)* a CARTS-independent TM cargo protein (VSVG). To that end, we
338 exchanged the lumenal domains (while maintaining the correct topology) of ST and VSVG for
339 that of TGN46, thereby generating two chimeric constructs: GFP-ST-TGN46lum, and GFP-
340 VSVG-TGN46lum, respectively (***Fig. 4A***). We then studied the intra-Golgi localization,
341 CARTS-mediated export selectivity, and Golgi export rate of these proteins in relation to their
342 WT counterparts. Our results indicate that GFP-ST-TGN46lum maintained a good degree of
343 colocalization with ST-mCherry and additionally it increased its colocalization with TGN46-
344 mRFP (***Fig. 4B*** and ***Fig. S7A***). Similar results were obtained for the intra-Golgi localization of
345 GFP-VSVG-TGN46lum with respect to TGN46-mRFP and VSVG-HA (***Fig. 4C*** and ***Fig.***
346 ***S7B***). As an additional control to eliminate any sources of possible intra-Golgi sorting signals
347 residing in the lumenal region of VSVG, we also included GFP-VSVG-Δlum – a deletion
348 mutant of VSVG lacking the lumenal domain (***Figure 4A***). This construct shows a reduced
349 colocalization with respect to both TGN46-mRFP and VSVG-HA, possibly indicating a tug-
350 of-war between lumenal signals – driving localization towards TGN46-positive export domains
351 – and TM/cytosolic signals – driving localization towards VSVG-positive export domains (***Fig.***
352 ***4C*** and ***Fig. S7B***). Despite these subtle differences in their intra-Golgi localization, the GFP-
353 VSVG-TGN46lum chimera specifically exits the TGN in CARTS, with a similar specificity to
354 that of TGN46-GFP, whereas GFP-VSVG-Δlum exits in VSVG carriers, similarly to VSVG-
355 GFP (***Fig. 4D*** and ***Fig. S8A***). In line with these observations, FLIP microscopy showed a fast
356 Golgi export rate of GFP-VSVG-TGN46lum, indistinguishable from that of GFP-TGN46 WT,
357 and a somewhat slower export rate for both GFP-VSVG-Δlum and VSVG-GFP (***Fig. 4F,G*** and
358 ***Fig. S9A,C,D***). These results indicate that the lumenal domain of TGN46 can re-direct other
359 TM cargo proteins into CARTS, thereby acting as a gain-of-function domain for fast export in
360 CARTS out of the Golgi apparatus. Similarly, fusing the lumenal domain of TGN46 to ST also

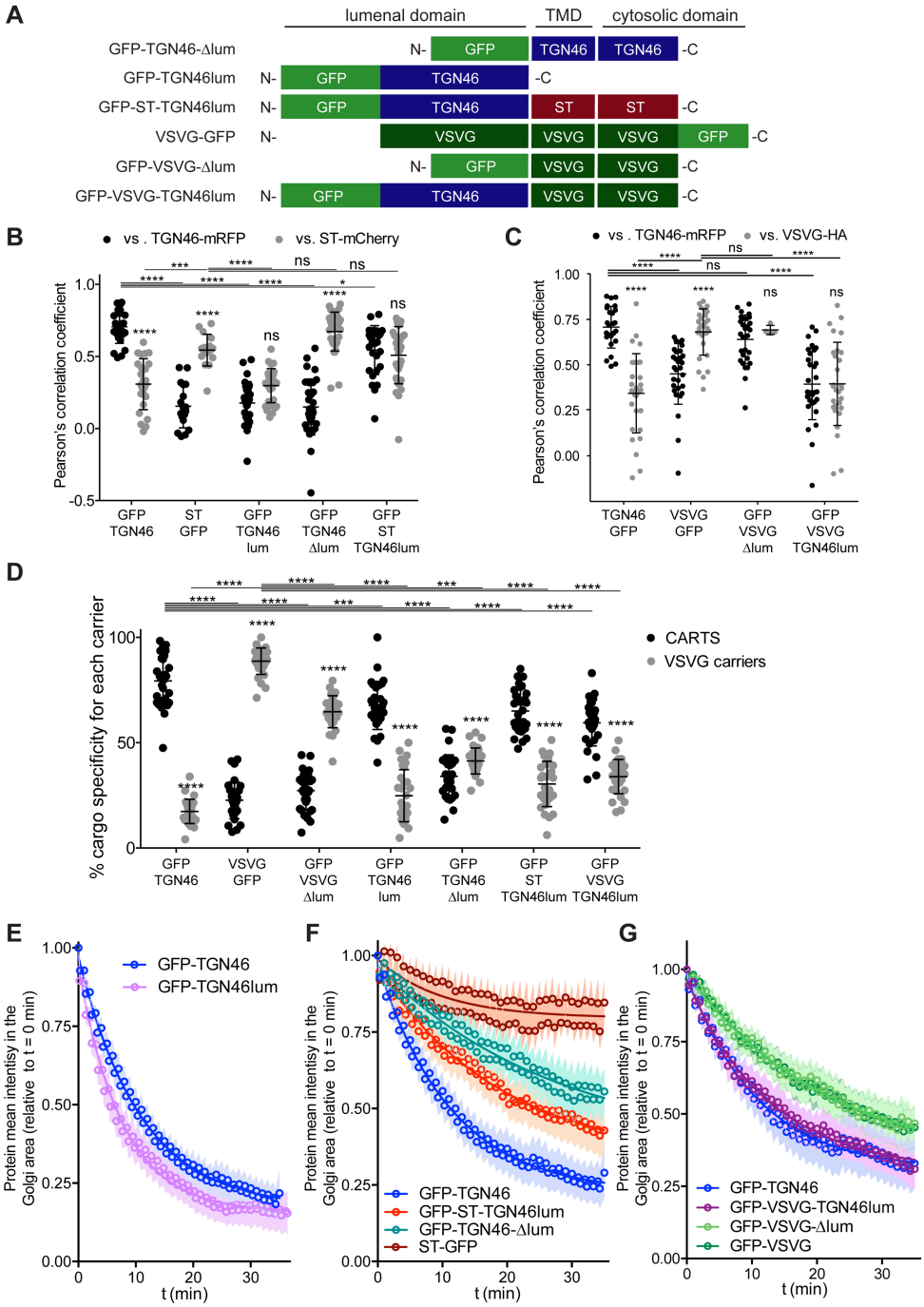

Figure 4. The lumenal domain of TGN46 is necessary and sufficient for its CARTS-mediated export from the TGN. **(A)** Schematic representation of construct domain topology. TMD: transmembrane domain. **(B)** Pearson's correlation coefficient between the perinuclear fluorescence signal of the x-axis indicated proteins with respect to TGN46-mRFP (black symbols) or ST-mCherry (gray symbols), measured from confocal micrographs of HeLa cells expressing the indicated proteins. Results are from at least 10 cells from each of n=3 independent experiments (individual values shown, with mean ± stdev). **(C)** Pearson's correlation coefficient between the perinuclear fluorescence signal of the x-axis-indicated proteins with respect to TGN46-mRFP (black symbols) or VSVG-HA (gray symbols; detected by immunofluorescence using an Alexa Fluor 647-conjugated secondary antibody), measured from confocal micrographs of HeLa cells expressing the indicated proteins. Results are from at least 10 cells from each of n=3 independent experiments (individual values shown, with mean ± stdev). **(D)** Percentage of transport carriers containing each of the cargoes described on the x-axis that are also positive for PAUF (CARTS, black symbols) or VSVG (VSVG carriers, gray symbols), as measured from confocal micrographs of HeLa cells expressing the indicated proteins. Results are from at least 10 cells from each of n=3 independent experiments (individual values shown, with mean ± stdev). **(E–G)** Relative fluorescence intensity average time trace (mean ± s.e.m.) of FLIP experiments for the indicated proteins. Symbols correspond to actual measurements, solid lines to the fitted exponential decays.

361 created an export-competent protein that exits the TGN by being specifically sorted into
362 CARTS (***Fig. 4D*** and ***Fig. S8A***). Remarkably, GFP-ST-TGN46lum has a shorter Golgi
363 residence time as compared to ST-GFP, with an export rate slightly slower but comparable to
364 that of GFP-TGN46 WT (***Fig. 4F*** and ***Fig. S9A,C***). Altogether, these results indicate that, as
365 long as the protein is correctly localized within the Golgi membranes, signals encoded in the
366 lumenal domain of TGN46 are not only necessary, but also *sufficient* for cargo sorting into
367 CARTS.

368 **Correlation between CARTS specificity and Golgi export rate of cargo proteins**

369 Our data thus far suggest that proeins with a high specificity for the CARTS export pathway
370 have a relatively fast Golgi export rate (***Figs. 2–4***). To quantitatively illustrate these findings,
371 we plotted for each of the tested cargo proteins their CARTS specificity as a function of their
372 Golgi residence time. The plots reveal the existence of a negative correlation between CARTS
373 specificity and Golgi residence time (slope~-0.9±0.4% min^{-1}, r^2~0.4) (***Fig. 5A***). Both TGN46
374 WT (***Fig. 5A***, dark green) and the different chimeric cargo proteins that contain the lumenal
375 domain but not the cytosolic tail of TGN46 (***Fig. 5A***, light green and light blue) are selectively
376 sorted into CARTS (>50% specificity) and rapidly exported out of the Golgi (short Golgi
377 residence times ~10–30 min). Interestingly, in the absence of the lumenal domain of TGN46
378 (***Fig. 5A***, red) or when only the TMD sequence of TGN46 is altered (while keeping the WT
379 cytosolic tail) (***Fig. 5A***, yellow), cargoes lost CARTS specificity (<35%) with the concomitant
380 decrease in the Golgi export rate (larger Golgi residence times ~30–50 min), consistent with
381 the values found for VSVG (***Fig. 5A***, blue), a cargo that is excluded from CARTS (Wakana et
382 al., 2012) and shows a slower Golgi export rate (Golgi residence time ~30 min). Taken together,
383 these data indicate that VSVG-containing carriers mediate a relatively slower Golgi export
384 route as compared to CARTS, thereby underscoring the different export kinetics of distinct
385 Golgi export routes.

386 **The cargo sorting function of TGN46 is mediated by its lumenal domain**

387 TGN46 is a bona fide CARTS component (Wakana and Campelo, 2021), and our data indicate
388 that it is required for PAUF sorting into CARTS for secretion (***Fig. 1***). Furthermore, we have
389 shown that the lumenal domain of TGN46 is necessary and sufficient for the incorporation of
390 this TM protein into CARTS (***Fig. 4***). Thus, it is plausible that TGN46 facilitates the sorting of
391 client cargoes via its lumenal domain. To test this hypothesis, we investigated whether the
392 expression of different mutants of TGN46 rescues the sorting and export defect we have
393 observed in TGN46-KO cells. In particular, we studied the following TGN46-based proteins:
394 GFP-TGN46 (wild type protein), GFP-TGN46-Δcyt (no cytosolic tail), GFP-TGN46-ST TMD
395 (TGN46 with the shorter TMD of the Golgi resident ST), and GFP-TGN46-Δlum (no lumenal

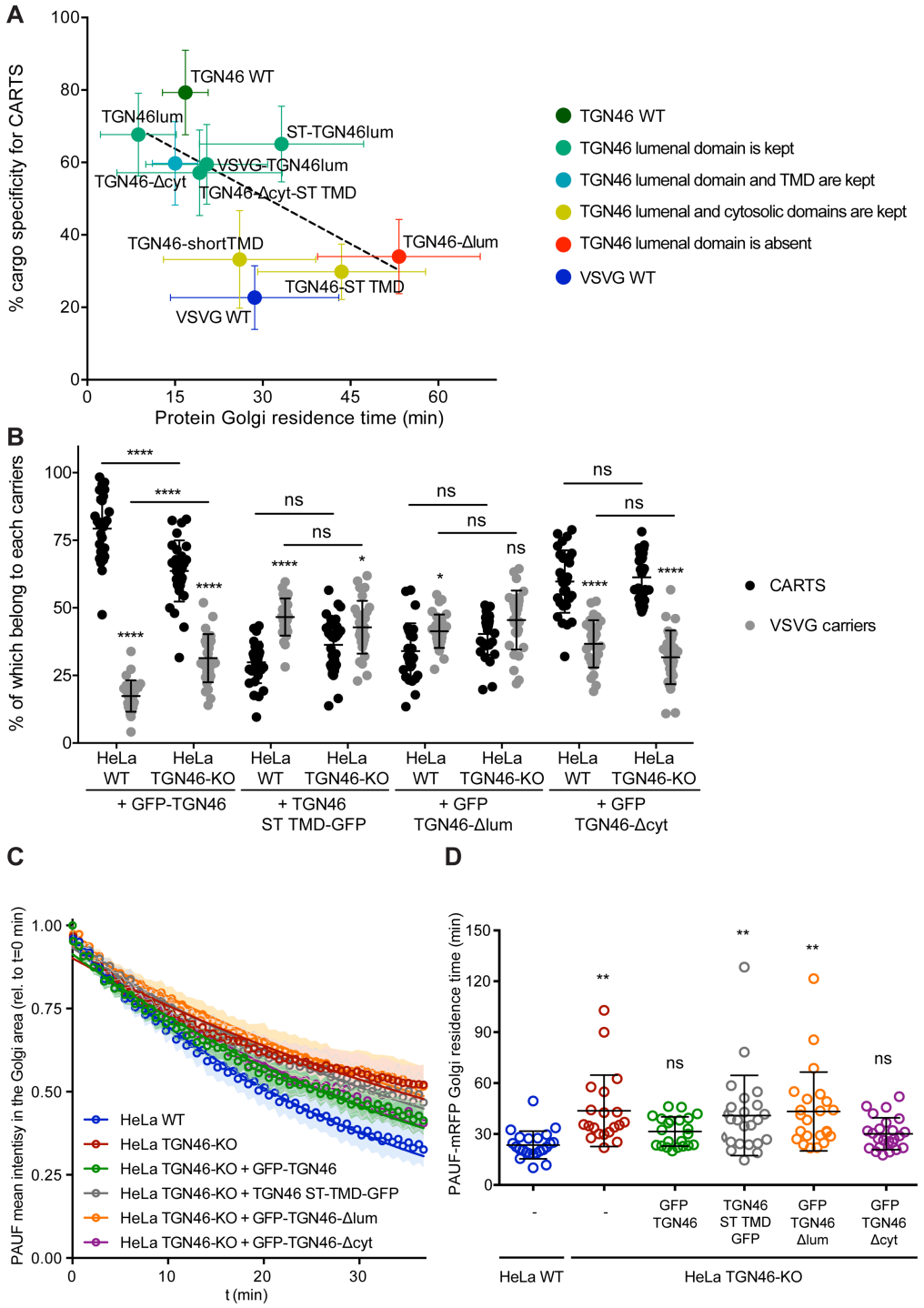

Figure 5. The cargo sorting function of TGN46 is mediated by its lumenal domain. (A) CARTS specificity of cargo proteins correlates with their Golgi export rate. Plot of the percentage of cargo-positive vesicles that are also positive for PAUF (CARTS marker) as a function of the Golgi residence time as measured from FLIP experiments, for the different indicated cargo proteins (color coding explained in the legend on the right). Dashed black line represents a linear fit of the data points (shown as mean ± s.e.m.), where the slope is statistically different from zero (extra sum-of-squares F test, p value= 0.04). **(B)** Percentage of transport carriers containing each of the cargoes described on the x-axis that are also positive for PAUF (CARTS, black symbols) or VSVG (VSVG carriers, gray symbols), as measured from confocal micrographs of HeLa cells (either WT or TGN46-KO cell lines) expressing the indicated proteins. Results are at least 10 cells from each of n=3 independent experiment (individual values shown, with mean ± stdev). **(C)** Relative fluorescence intensity average time trace (mean ± s.e.m.) of FLIP experiments for the indicated proteins expressed in HeLa WT or HeLa TGN46-KO cells, as detailed in the legend. Symbols correspond to actual measurements, solid lines to the fitted exponential decays. **(D)** Residence time of PAUF-mRFP in the perinuclear area of HeLa cells (WT or KO), expressing the different proteins as labeled in the x axis, and measured as the half time of the FLIP curves. Results are from 7–12 cells from each of n=3 independent experiments (individual values shown, with mean ± stdev).

396 domain). First, TGN46-KO cells co-expressing any of these TGN46 constructs together with
397 PAUF-mRFP or VSVG-HA were synchronized by a 20º block and 15 min release at 37º, after
398 which the cells were fixed and prepared for fluorescence microscopy (***Fig. S10A***). We
399 quantified the percentage of carriers containing the different TGN46 mutants that were also
400 positive for either PAUF-mRFP (CARTS marker) or VSVG-HA (non-CARTS marker) and
401 compared those to the distributions found when the same proteins were expressed in the
402 parental HeLa cells (***Fig. 5B***; see also ***Fig. 2C, 3C, 4D***). Our results indicate that CARTS
403 selectivity of these cargo proteins was not severely altered in the TGN46 KO cells as compared
404 to the parental cell line. Next, we carried rescue experiments by performing FLIP in TGN46-
405 KO cells expressing PAUF-mRFP together with GFP-TGN46, GFP-TGN46-Δcyt, TGN46-ST
406 TMD-GFP, or GFP-TGN46-Δlum to measure the rate of PAUF-mRFP export from the Golgi.
407 Interestingly, overexpression of GFP-TGN46 WT or GFP-TGN46-Δcyt – but not of TGN46-
408 ST TMD-GFP or GFP-TGN46-Δlum – was able to rescue PAUF-mRFP export from the Golgi
409 in TGN46-KO cells (***Figs. 5C,D*** and ***S11***). Taken our data together, we propose a model in
410 which the proper partitioning of TGN46 into TGN export domains (sites of CARTS biogenesis)
411 is required for its lumenal domain to efficiently recruit and sort PAUF and possibly other
412 CARTS cargoes into nascent transport carriers for secretion.

413

414 **DISCUSSION**

415 **TGN46 is necessary for cargo loading into CARTS**

416 Here, we revealed a novel role for TGN46 in the sorting of the secretory cargo protein PAUF
417 into nascent transport carriers at the TGN. CRISPR/Cas9-edited HeLa cells lacking TGN46
418 showed *(i)* a drastic inhibition in PAUF secretion (***Fig. 1A***); *(ii)* a reduction in the number of
419 cytoplasmic CARTS – but not of other TGN-to-PM carriers such as VSVG carriers – (***Fig. 1B***);
420 and *(iii)* a decrease in the Golgi export rate of PAUF (***Fig. 1C,D***). To investigate the role of
421 TGN46 in TGN export, we took advantage of the phenotype created by the exogeneous
422 expression of PKD-KD, which consists in the presence of long, cargo-containing tubules
423 emanating from the TGN membranes (Liljedahl et al., 2001). Because these tubules are fission-
424 defective transport carriers, and membrane fission is downstream of cargo sorting, we could
425 use this assay as a useful approach to investigate cargo sorting into PKD-dependent transport
426 carriers at the TGN. Our results showed that TGN46 is not necessary for membrane tubulation
427 but it is essential to sort and package the secretory cargo PAUF into PKD-KD-induced TGN
428 tubules (***Fig. 1E***), therefore suggesting a prime role of TGN46 in cargo sorting. Indeed, TGN46
429 (and its rodent orthologs TGN38/TGN41) had previously been suggested to act as a cargo
430 receptor, based on the fact that this protein shares the characteristics of a typical cargo receptor:

431 it is a type-I single-pass TM protein that cycles between the TGN and the PM (Stanley and
432 Howell, 1993). Although future work will be necessary to pinpoint the mechanism that TGN46
433 uses for cargo sorting and loading into carriers, we believe that the data reported here shed
434 some light into the actual role of human TGN46 for the sorting and loading of cargo proteins
435 into TGN-derived transport carriers destined to the cell surface.

436 Although in here we have focused on the study of the model CARTS cargo protein PAUF, it
437 seems reasonable to expect that TGN46 is responsible for the sorting of other CARTS cargoes.
438 Interestingly, the lumenal domain of TGN38 has been shown to interact with the adhesion
439 receptor integrin $ß_1$ and to partially co-localize with integrins α_5 and $ß_1$, but not α_V or $ß_3$ (Wang
440 and Howell, 2000). In addition, TGN38 regulates cell adhesion, as the overexpression of
441 TGN38 leads to cell detachment from the substrate (Luzio et al., 1990; McNamara et al., 2004;
442 Lee and Banting, 2002; Humphrey et al., 1993; Reaves et al., 1993). Remarkably, integrin $ß_1$ is
443 transported from the TGN to the cell surface in a Rab6-mediated (Huet-Calderwood et al.,
444 2017) and PKD-dependent manner (Yeaman et al., 2004). Because TGN46 binds a cytosolic
445 protein complex made of 62 kDa protein (p62) and Rab6 (Jones et al., 1993), and CARTS are
446 PKD-dependent transport carriers that share many similarities with Rab6-positive carriers
447 (Wakana and Campelo, 2021), we propose that the observed role of TGN46 as a cargo receptor
448 for the sorting of the soluble CARTS-specific cargo PAUF is quite general, and can include a
449 long list of both soluble and TM cargo proteins, such as $\alpha_5ß_1$ integrins. In addition, TGN46 has
450 been recently reported to assist in the trafficking of severe acute respiratory syndrome
451 coronavirus 2 (SARS-CoV-2), as this protein is upregulated in SARS-CoV-2-infected cells and
452 cells depleted of TGN46 showed a reduced SARS-CoV-2 infection rate (Zhang et al., 2022).
453 In summary, further work will be required to grasp the full magnitude of the role of TGN46 in
454 protein sorting for export and secretion out of the TGN, which can provide ideas to help in the
455 rational design of new therapeutic tools to target human pathologies associated with secretion
456 defects.

457 **TGN46 localization to *trans*-Golgi membranes is independent of TMD length and**
458 **composition**

459 Different mechanisms that mediate the spatial and temporal organization of Golgi residents
460 (e.g., glycosylation enzymes) and their respective substrates (e.g., secretory cargoes) have been
461 proposed (Banfield, 2011; Welch and Munro, 2019; Lujan and Campelo, 2021). Amongst these,
462 a lipid-based retention/sorting mechanism has been proposed for Golgi TM proteins (Patterson
463 et al., 2008; Munro, 1991; Sharpe et al., 2010; Munro, 1995; Lippincott-Schwartz and Phair,
464 2010). This mechanism builds on the observation that the levels of certain lipids, such as
465 cholesterol and SM, are enriched along the *cis*- to *trans*- axis of the Golgi stack (Van Meer et

466 al., 2008; Bretscher and Munro, 1993). This lipid gradient correlates with an increase in the
467 thickness of those membranes (Mitra et al., 2004). In addition, a comprehensive bioinformatic
468 study using large datasets of TM proteins from different organisms showed a correlation
469 between the intracellular localization of these proteins and different specific features of their
470 TMDs, such as their length, which on average is shorter for proteins of the early secretory
471 pathway as compared to those of the late secretory pathway (Sharpe et al., 2010). Furthermore,
472 it has been proposed that not only the TMD length but also the distribution of bulky and highly
473 hydrophobic amino acids within the TMD affect the specific location of TM proteins (Sharpe
474 et al., 2010; Quiroga et al., 2013). Altogether, these studies have led to the suggestion of the
475 hydrophobic matching model, which proposes that gradients in bilayer thickness along the
476 membranes of the secretory pathway contribute/drive the sorting and retention of TM proteins
477 across the secretory pathway. Although there is compelling evidence for a TMD-based
478 mechanism for targeting certain TM proteins to specific cell surface domains (Milovanovic et
479 al., 2015), to localize type-II resident proteins of the cell surface and the Golgi membranes
480 (Munro, 1995; Quiroga et al., 2013), and also to sort the type-III TM protein linker for
481 activation of T-cells (LAT) by raft-mediated partitioning (Diaz-Rohrer et al., 2014; Lorent et
482 al., 2017; Castello-Serrano et al., 2023), it remained unclear how this mechanism contributed
483 to the retention, sorting and lateral segregation of Golgi resident enzymes and their substrates.
484 Interestingly, by using a coarse-grained mathematical model of intra-Golgi transport, Dmitrieff
485 et al. showed that experimental data on the Golgi dynamics of secretory cargoes and Golgi
486 residents cannot be explained if the hydrophobic matching mechanism is the sole retention
487 mechanism for Golgi residents (Dmitrieff et al., 2013). In agreement with this latter proposal,
488 our results revealed that hydrophobic mismatch between TMDs and bilayer thickness is not
489 sufficient to drive the sorting of a TM Golgi-resident enzymes from substrate cargoes along the
490 *trans*-Golgi/TGN membranes. Specifically, we studied the role of TMD length and amino acid
491 composition in intra-Golgi localization of the type-I single-pass TM cargo glycoprotein
492 TGN46, and observed that localization and sialylation of TGN46 is not affected when its TMD
493 is shortened or even replaced by that of the Golgi-resident type-II TM enzyme ST (***Fig. 3A,B***
494 and ***Fig. S3A***). These data suggest that the hydrophobic length and amino acid composition of
495 the TMD of TGN46 is not a major contributing factor to localize this TM protein into Golgi
496 export domains for its function in sorting and packaging of soluble cargoes into nascent
497 CARTS.

498 **A role for the cytosolic tail of TGN46 in driving its proper intra-Golgi localization**

499 Our results indicate that the cytosolic tail of TGN46 contains a specific signal allowing the
500 perinuclear pool of TGN46 to localize in the right sub-compartment within the TGN
501 membranes. In particular, the localization of a TGN46 mutant lacking the cytosolic tail was

502 shifted towards Golgi processing domains (ST enzyme-positive regions) rather than in export
503 domains (TGN46 WT-positive regions) (***Fig. 2B*** and ***Fig. S2A***). It has been well documented
504 that the cytosolic tail of TGN38 – the rodent ortholog of TGN46 – contains a tyrosine-based
505 motif for internalization and recycling of the protein back to the TGN (Bos et al., 1993;
506 Humphrey et al., 1993). Adding to these earlier reports, our data suggest that the cytosolic tail
507 of TGN46 also determines its fine intra-Golgi localization. Factors such as Vps74/GOLPH3 or
508 coat proteins such as COPI (Tu et al., 2008; Wood et al., 2009; Welch et al., 2021), influence
509 enzyme-cargo interaction/segregation by recognizing cytoplasmic signals and thereby inducing
510 protein retention by fast recycling. In addition, SM metabolism can also contribute to laterally
511 organize the Golgi membranes at the nanoscale for efficient cargo-enzyme interactions (Duran
512 et al., 2012; van Galen et al., 2014).

513 **Cargoes destined for secretion exit the Golgi with different export rates**

514 We observed that the Golgi residence time of different TGN46-based chimeric proteins was
515 different depending on the specific export route they use to exit the TGN (***Fig. 5A***). In
516 particular, when we compared the export rate of two different PKD-dependent TM proteins
517 (TGN46, which is exported in CARTS; and VSVG, which is not), we found that CARTS appear
518 to be a faster export route (~15 min Golgi residence time) than VSVG carriers (~30 min Golgi
519 residence time) (***Fig. 5A***). Remarkably, when we generated a series of chimeras combining
520 different domains from different proteins, we observed that loss of CARTS specificity
521 correlated with larger Golgi residence times (***Fig. 5A***). These results could provide an
522 explanation as to why cells use different routes (with different machineries) for the export of
523 secretory or TM cargo proteins to the same destination, *i.e.*, different cargoes might require
524 longer/shorter residence times in the Golgi and/or faster transport kinetics to the cell surface. It
525 is possible that developing various TGN-to-PM export routes of different kinetics might have
526 endowed cells with beneficial mechanisms to cope with their secretory needs under stress
527 conditions.

528 CARTS have been suggested to be enriched in cholesterol and SM (Wakana et al., 2021;
529 Wakana and Campelo, 2021), and their biogenesis to require intact ER-Golgi membrane
530 contact sites (MCS) supplying the TGN with these lipids (or their precursors) (Wakana et al.,
531 2015, 2021). Notably, data from Deng, Pakdel et al. suggested that TGN46 is a native cargo of
532 the SM-dependent TGN export pathway, as it was identified by mass spectrometry to be co-
533 packaged in carriers containing the lumenal SM sensor EQ-SM-APEX2 (Deng et al., 2018).
534 Given the similarities between the SM/Cab45 and CARTS export pathways (Stalder and
535 Gershlick, 2020; Wakana and Campelo, 2021), it is tempting to speculate that TGN46 could be

536 enriched in ER-Golgi MCS and perhaps complement the sorting function of Cab45 for a subset
537 of secretory cargo proteins.

538 Further elaborating on these specific needs/characteristics of different cargoes/export routes
539 will be of outmost importance in the future to better understand the intricate relationships
540 between physiological needs and the regulation of the secretory machinery of the cell (Di
541 Martino et al., 2019; Luini and Parashuraman, 2016; Cancino et al., 2013; Wakana and
542 Campelo, 2021).

543

544 **IDEAS AND SPECULATIONS**

545 In the following, we would like to propose some ideas and speculate on a possible mechanism
546 by which TGN46 could serve as a cargo sorting factor at the TGN.

547 **The lumenal domain of TGN46 can form liquid condensates *in vitro***

548 Our data suggest that the lumenal domain of TGN46 might have a propensity to self-associate,
549 because *(i)* the steady-state intra-Golgi localization of TGN46 is lost when the lumenal domain
550 is deleted (***Fig. 4B*** and ***Fig. S7A***); and *(ii)* although the soluble lumenal domain of TGN46
551 showed an intermediate intra-Golgi localization phenotype, anchoring this domain to the
552 membrane by fusing it to the *trans*-Golgi-targeting sequence of ST conferred this chimera a
553 localization pattern indistinguishable from that of full length TGN46 (***Fig. 4B*** and ***Fig. S7A***).
554 To obtain insights on how this might occur, we analyzed the sequence features of the lumenal
555 domain of TGN46 (***Fig. S12A***). On the one hand, TGN46 is a heavily glycosylated protein,
556 including 9 predicted *N*-linked glycosylation sites, multiple *O*-linked glycosylation sites, as
557 well as 5 phosphosites (***Fig. S12B***), all of them located at the lumenal domain. Structurally,
558 this region is highly disordered, as evidenced by a high PONDR score (in the range 0.5–1) for
559 most of its amino acid sequence (***Fig. S12C***), indicating with high probability that the lumenal
560 domain of TGN46 is an essentially intrinsically disordered region (IDR). In recent years, IDR
561 of various proteins have been shown to have the capacity to form biomolecular condensates
562 (Banani et al., 2017; Garcia-Cabau and Salvatella, 2021; Shin and Brangwynne, 2017; Hyman
563 et al., 2014; Brangwynne et al., 2009; Case et al., 2019; Mittag and Pappu, 2022). Due to their
564 liquid nature, these condensates take spherical shapes, and their components are mobile within
565 the condensate (dense phase) and can also exchange with those present, at a lower
566 concentration, in the external solution (light phase). We thus tested whether the TGN46 lumenal
567 domain has the capacity to form liquid droplets *in vitro*. We purified the protein domain (amino
568 acids 1–437) fused to GFP in *E. coli*, as this renders the simplest form of TGN46 lumenal
569 domain (without glycosylations). We assessed by fluorescence microscopy the formation of

570 liquid droplets at different protein concentrations and with or without the addition of Ficoll – a
571 well-known crowding agent used to mimic the crowded environment of the Golgi lumen. Our
572 results indicate that, when present at a high concentration (100 μM) and in the presence of
573 Ficoll, TGN46-lumenal is able to form spherical structures of a range of sizes (~1 μm),
574 characteristic of biomolecular condensates (***Fig 6A***). Notably, time-lapse fluorescence
575 microscopy imaging revealed fusion events between droplets, which is indicative of their liquid
576 nature (***Fig. 6B***). In addition, we carried out fluorescence recovery after photobleaching
577 (FRAP) experiments to determine whether protein molecules could diffuse inside the droplets.
578 Our results indicate that, indeed, protein molecules diffuse within the dense phase and that the
579 fluorescence recovers with a characteristic half-time of 4.46±1.54 s, and a mobile fraction (MF)
580 of 0.70±0.11 (***Fig. 6C***); we also performed FRAP experiments where an entire droplet was
581 bleached and observed fluorescence recovery indicating that protein molecules do exchange
582 between the light and dense phases (***Fig. 6D***). Together, these results show the capacity of the
583 TGN46 lumenal domain to form liquid droplets *in vitro*. We further characterized the driving
584 forces for this process by assessing the effect of solution conditions on phase separation. We
585 first studied the effect of addition of NaCl to the samples (***Fig. 6E***), and found that this
586 decreases the propensity of the domain to phase separate, indicating that droplet formation is
587 favored at low ionic strength. These data suggest that the interactions stabilizing the droplets
588 formed by TGN46 are of electrostatic nature, between amino acid side chains of opposite
589 charge or hydrogen bonds. This behavior is in agreement with a clear bias in the residue type
590 composition of the domain, that is highly enriched in Lys and Glu relative to a typical ID
591 domain as defined by the DisProt 3.4 database (***Fig. S12D–F***). Finally, we assessed the effect
592 of temperature on droplet formation by measuring the apparent absorbance, *i.e.,* the turbidity,
593 of the same samples at 20, 40 and 60 ºC (***Fig. 6F***), and obtained that the formation of liquid
594 droplets is promoted at high temperatures, in the lower critical solution temperature (LCST)
595 regime, indicating that *in vitro* droplet formation is entropy-driven. Taken together, our data
596 reveal that the lumenal domain of TGN46, which is crucial for its cargo sorting function, has
597 the capacity to form liquid droplets *in vitro*. This observation suggests a possible biophysical
598 mechanism for how this TM protein, by forming condensates in a cellular context, could
599 mediate the sorting of secretory cargoes into transport carriers for their secretion. Naturally,
600 these ideas still remain highly speculative but they help us ask a number of interesting
601 questions. First, what is the role of TGN46 lumenal domain glycosylation in the regulation of
602 droplet/condensate formation? Also, we observed that phase separation of non-glycosylated
603 TGN46 lumenal domain is promoted at relatively high protein concentration (100 μM) and in
604 the presence of the crowding agent Ficoll. These conditions might seem at first glance
605 somewhat extreme, however, we need to stress the fact that TGN46 is a TM protein and that

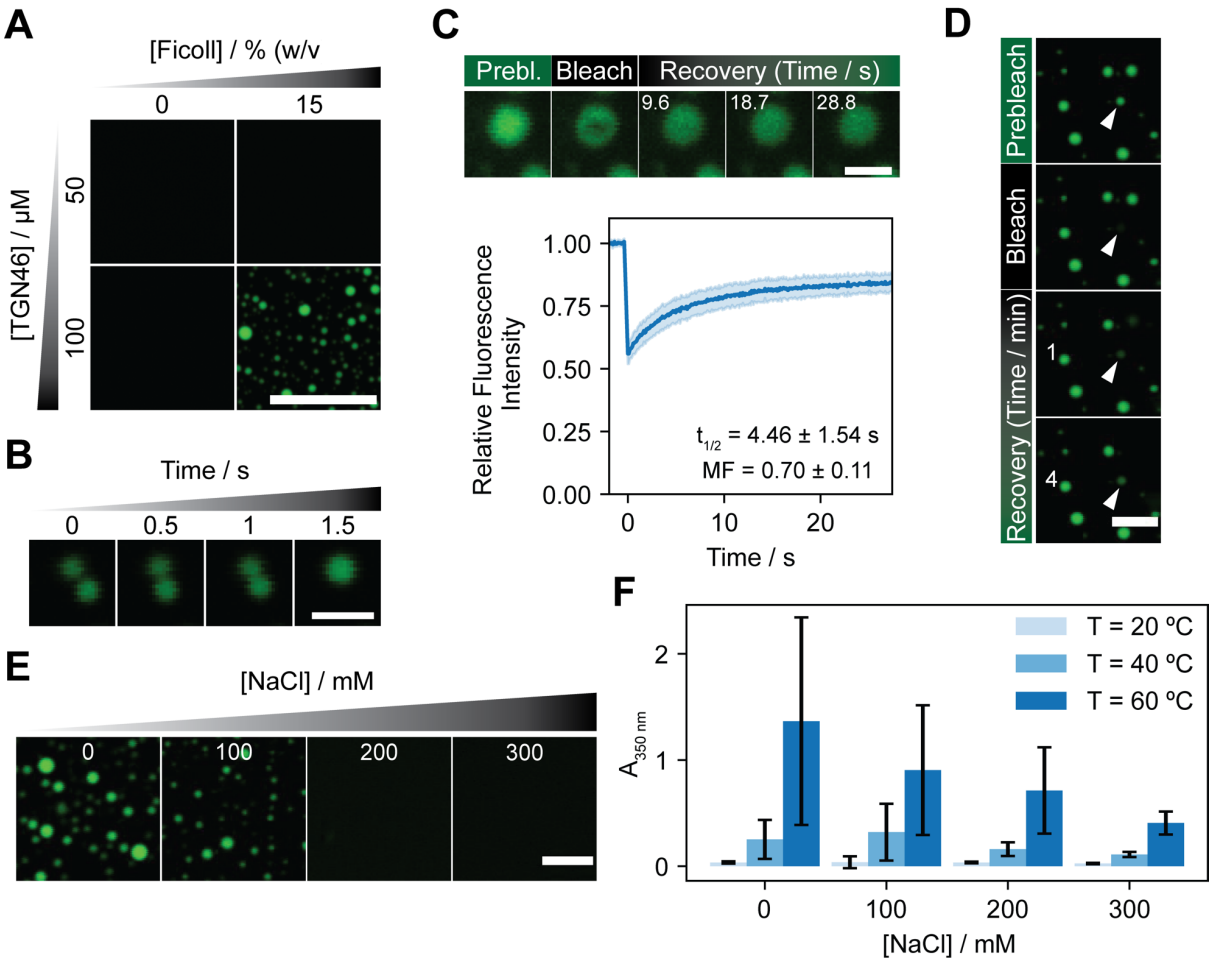

Figure 6. *In vitro* characterization of TGN46 lumenal domain condensate formation. (A) Fluorescence microscopy images of 50 and 100 µM protein concentration with 0 and 15 % (w/v) Ficoll 70 at 40 ºC. Scale bar represents 10 µm. **(B)** Example of a fusion event. Scale bar represents 2 µm. **(C)** FRAP experiment showing recovery after photobleaching within a single droplet. Scale bar represents 2 µm. The FRAP curve shown as the mean and standard deviation of 20 independent measurements and the corresponding fitted values are shown in the bottom plot. **(D)** FRAP experiment showing recovery after photobleaching of an entire droplet. Scale bar represents 5 µm. **(E)** Fluorescence microscopy images at different ionic strengths (0, 100, 200 and 300 mM NaCl) of a 100 µM TGN46lum sample with 15 %(w/v) Ficoll 70 at 40 ºC. Scale bar represents 5 µm. **(F)** Apparent absorbance measurements at 350 nm of the same samples as **(E)** at temperatures of 20, 40 and 60 ºC.

606 condensation of TM proteins by can be assisted by a local nucleation that locally increases the
607 protein concentration (Garcia-Cabau and Salvatella, 2021; Case et al., 2019). Interestingly, the
608 levels of the cation-dependent mannose 6-phosphate receptor – a well-known cargo receptor at
609 the TGN for the sorting of lysosomal hydrolases into clathrin-coated vesicles – are about 10-
610 fold higher than those of TGN46: ~200,000 copies vs. ~30,000 copies, respectively, per HeLa
611 cell (Kulak et al., 2014). Of notice, our co-immunoprecipitation experiments showed no
612 evidence for strong TGN46-TGN46 protein interactions (***Fig. S6C***), which agrees with our
613 suggestion that TGN46 forms biomolecular condensates that are stabilized by weak
614 interactions. It is therefore tempting to speculate that the mechanism of cargo sorting by TGN46
615 might be different from that of a classical cargo receptor, such as the mannose 6-phosphate
616 receptor, which binds its clients in an ~1:1 stoichiometry. It still remains unknown whether
617 PAUF is recruited to nascent CARTS by the lumenal domain of TGN46. PAUF is a putative
618 lectin, so it is possible that it interacts with TGN by recognizing the glycans on its lumenal
619 domain (***Fig. S12B***). Alternatively, or in parallel, TGN46 condensates could be liquid droplets
620 with a specific chemical microenvironment (pH, Ca^{2+} concentration, etc.), which might serve
621 to recruit certain cargoes. Future endeavors along these lines will help elucidate the mechanistic
622 details of cargo sorting by TGN46.

623 Remarkably, Parchure et al. recently showed that liquid-liquid phase separation (LLPS) might
624 also play a dominant role in the formation of secretory insulin-containing granules for regulated
625 exocytosis (Parchure et al., 2022). The authors showed that the chromogranins – key regulators
626 of secretory granule formation – can undergo LLPS *in vitro* in conditions of low pH, such as
627 the one found in the TGN. Notably, cargoes such as proinsulin or LyzC do co-partition with
628 chromogranins in liquid droplets, and put forward a "client sponge" model in which secretory
629 cargoes would be sorted into liquid biomolecular condensates based on their size. It will be
630 interesting to investigate whether the TM protein TGN46 and soluble chromogranins use two
631 parallel condensation-based pathways for the sorting of different cargoes for constitutive and
632 regulated secretion, respectively.

633

634 **CONCLUSION**

635 In summary, we presented here experimental results that support a model in which TGN46
636 serves as a sorting receptor for a subset of cargoes at the TGN. Thanks to TGN46, these cargoes
637 are sorted packaged into nascent CARTS for their fast delivery to the cell surface or for
638 secretion outside the cell. The sorting capabilities of TGN46 are ascribed to its lumenal domain,
639 an IDR prone to undergo phase separation. Indeed, our *in vitro* results showed that this domain
640 has the capability to form liquid droplets. Based on our findings, we propose a working model

641 in which TGN46 forms small biomolecular condensates at the TGN that serve to recruit
642 secretory cargoes in the lumen of the TGN for their sorting and fast export to the cell surface
643 by CARTS.

644

645 **ACKNOWLEDGMENTS**

646 We thank members of the Single Molecule Biophotonics lab at ICFO, Chris Burd, Ivan
647 Castello-Serrano, and Ilya Levental for valuable discussions. We thank Hideaki Sugiura (Tokyo
648 University of Pharmacy and Life Science) for performing preliminary experiments. We thank
649 Nathalie Brouwers and the Centre for Genomic Regulation/Universitat Pompeu Fabra FACS
650 Unit (Barcelona) for help with cell sorting and the IRB Barcelona Advanced Digital
651 Microscopy (ADM) Core Facility for help with microscopy. We also thank Jordi Andilla and
652 Maria Marsal for technical support at the Super-resolution Light Nanoscopy (SLN) facility at
653 ICFO. The authors acknowledge the Protein Technologies Unit, Centre for Genomic
654 Regulation (CRG) (Barcelona, Spain) for providing the protein used in this study. C.G.-C.
655 acknowledges a FPI fellowship awarded by MINECO in the 2018 call. P.L., J.V.L., X.S.,
656 M.F.G.-P. and F.C. acknowledge support from the Government of Spain (FIS2015-63550-R,
657 BFU2015-73288-JIN, FIS2017-89560-R, RYC-2017–22227, PID2019-106232RB-
658 I00/10.13039/501100011033/110198RB-I00 and PID2020-113068RB-I00 /
659 10.13039/501100011033; Severo Ochoa CEX2019-000910-S), Fundació Privada Cellex,
660 Fundació Privada Mir-Puig, and Generalitat de Catalunya (CERCA, AGAUR), ERC
661 Consolidator Grant CONCERT (GA 648201) and Advanced Grants NANO-MEMEC (GA
662 788546) and LaserLab 4 Europe (GA 654148).

663

664 **AUTHOR CONTRIBUTIONS**

665 Conceptualization, P.L. and F.C.; Methodology, P.L., C.G.-C., Y.W., J. V. L., C.R, X.S., and
666 F.C.; Software, C.R.; Formal analysis, P.L., C.G.-C., Y.W., C.R., X.S., V.M., M.F.G.-P., and
667 F.C.; Investigation, P.L., C.G.-C., Y.W., J. V. L., and F.C.; Writing – Original Draft, P.L. and
668 F.C.; Writing – Review & Editing, all authors; Funding Acquisition, V.M., X.S., M.F.G.-P.,
669 and F.C.; Supervision, X.S., M.F.G.-P., and F.C.

670

671 **DECLARATION OF INTERESTS**

672 The authors declare no competing interests

673 **METHODS**

674 **Reagents and antibodies**

675 Brefeldin-A (BFA), from Sigma-Aldrich, was dissolved in Dimethyl Sulfoxide (DMSO)
676 (Sigma-Aldrich) as a 10 mg/mL stock solution, and used at 5 µg/ml concentration. N-
677 Hexanoyl-D-erythro-sphingosine (D-cer-C6), from Matreya, was dissolved in pure ethanol
678 (Merck) as a 10 mM stock solution, and used at 20 µM concentration. Cycloheximide was
679 purchased from A.G. Scientific, diluted to 1M in DMSO as a stock solution, and used at 100
680 µM concentration. Ficoll 70 was purchased from Sigma-Aldrich and dissolved in water to a
681 64% (w/v) as a stock solution. NaCl was obtained from Melford. For the coating of the slides,
682 toluene was used from PanReac, ethanol from Scharlau and 3-
683 [methoxy(polyethyleneoxy)propyl]trimethoxysilane (CAS 65994-07-2) from acbr GmbH.
684 Sheep anti-human TGN46 was from AbD Serotec. Mouse monoclonal against HA was from
685 Biolegend. Mouse monoclonal against Myc was from Sigma-Aldrich. Rabbit polyclonal
686 antibody against Flag was from Sigma-Aldrich. Rabbit polyclonal antibody against GFP was
687 from Abcam. Alexa Fluor-labeled secondary antibodies were from Invitrogen and HRP-
688 conjugated secondary antibodies from Sigma-Aldrich. For STORM, the activator/reporter dye-
689 conjugated secondary antibodies were in-house-labelled donkey-anti-mouse and donkey-anti-
690 rabbit obtained from ImmunoResearch, used at a final concentration of 20 µg/ml. The dyes
691 used for labelling were NHS ester derivatives: Alexa Fluor 405 Carboxylic Acid Succinimidyl
692 Ester (Invitrogen), Cy3 mono-Reactive Dye Pack (GE HealthCare), and Alexa Fluor 647
693 Carboxylic Acid succinimidyl Ester (Invitrogen). Antibody labelling reactions were performed
694 as previously reported (Borgman et al., 2020).

695 **Cell culture, plasmids and siRNA**

696 HeLa cells were cultured in DMEM (Lonza and Capricorn Scientific) containing 10% fetal
697 bovine serum (FBS) (ThermoFisher and Capricorn Scientific), 1% penicillin/streptomycin
698 (Biowest), and 2 mM L-Glutamine (Biowest). Cells were transfected with DNA using Xtreme-
699 GENE 9 DNA (Roche) or with TransIT-HeLaMonster (Mirus) following manufacturer's
700 recommendations. The TGN46-GFP plasmid, which was kindly provided by Dr. S.
701 Ponnambalam (Leeds University, Leeds, England, UK), was generated by inserting human
702 TGN46 cDNA into a pEGFP-N1 vector using the BamHI restriction site. TGN46 ΔAAIL-GFP,
703 TGN46-ST TMD-GFP, GFP-TGN46, GFP-TGN46 LT, GFP-TGN46 TC, GFP-TGN46lum,
704 GFP-TGN46lum-ST TMD, GFP-TGN46lum-ST TC, GFP-TGN46lum-VSVG TC, and GFP-
705 VSVG TC were sub-cloned by Gibson assembly (Gibson et al., 2009) and/or DNA digestion
706 and ligation using TGN46-GFP as a backbone and TGN46-GFP, ST-GFP, or VSVG-GFP as
707 DNA sequence providers. TGN46-mRFP was generated by Gibson assembly of the KpnI- and

708 EcoRI-digestion of the previously described plasmid PAUF-mRFP (Wakana et al., 2012).
709 TGN46-ST TMD-mCherry was sub-cloned by Gibson assembly using TGN46-mRFP as the
710 backbone and ST-GFP as DNA sequence providers. PAUF-MycHis and PAUF-mRFP
711 plasmids were described earlier (Wakana et al., 2012). ST-GFP, which encodes for the initial
712 45 amino acids of the ST6Gal-I ST, comprising the cytosolic domain, the TMD and 20 amino
713 acids of the lumenal domain, was cloned into pEGFP-N1 as previously described (Duran et al.,
714 2012). The ST-mCherry plasmid was generated from the previously described plasmid ST-
715 FKBP-mCherry (Pecot and Malhotra, 2004) by Gibson assembly of the BglII- and BamHI-
716 digested plasmid. The VSVG-GFP plasmid was described previously (von Blume et al., 2009).
717 VSVG-HA was generated by Gibson assembly from VSVG-GFP. PKD2-KD-Flag plasmid was
718 described earlier (Bossard et al., 2007). pETM14-6his-mGFP -TGN46lum plasmid for bacterial
719 expression was cloned using a synthetic fragment of bacterial optimized TGN46 (gblock IDT),
720 meGFP amplified from GFP-TGN46-lum and assembled in pETM14 backbone vector using
721 Gibson assembly. All plasmids were verified by sequencing (STAB vida). SnapGene software
722 (obtained from GSL Biotech) and ApE software (by M. Wayne Davis) were used for molecular
723 cloning procedures.

724 For TGN46 transient silencing, HeLa cells were transfected using HiPerFect Transfection
725 Reagent (QIAGEN) with 5 nM of TGN46 siRNA (oligo name: SASI_HS01_00080765, from
726 Sigma-Aldrich), following the manufacturer's recommendations. MISSION siRNA Universal
727 Negative Control #1 was used as a control siRNA. 48h after transfection, corresponding
728 experiments were performed.

729 Single-clone TGN46 KO HeLa cells were generated by CRISPR/Cas9. HeLa cells were
730 transfected with U6-gDNA (5'-AAAGACGTCCCTAACAAGT-3'; clone ID es:
731 HSPD0000063884): CMV-eCas9-2a-tGFP (Sigma-Aldrich). 48h after transfection, GFP-
732 positive cells were sorted as individual cells by FACS using a BD Influx cell sorter (BD
733 Biosciences). Upon clone expansion, KO effectiveness of the different clones was checked by
734 SDS-PAGE and Western blotting and also by immunofluorescence microscopy.

735 **Immunofluorescence microscopy**

736 Samples were fixed with 4% formaldehyde in PBS for 15 min and permeabilized and blocked
737 with 0.2% Triton X-100, 3% BSA in PBS for 30 min prior to antibody staining. Fixed samples
738 were analyzed with a TCS SP8 STED 3X system (Leica) in confocal mode using a 100x 1.4NA
739 objective and HyD detectors. Images were acquired using the Leica LAS X software and
740 converted to TIFF files using ImageJ (version 1.43; National Institutes of Health). Two-channel
741 colocalization analysis was performed using the ImageJ software and the Pearson's correlation
742 coefficient was calculated in a ROI using the "Manders Coefficients" plugin developed at the

743 Wright Cell Imaging Facility (Toronto, Canada). The ROI was determined as a mask created
744 on the Golgi region formed upon Binary transformation (using the Default Thresholding given
745 by the software) of the sum of both channels. Vesicle colocalization analysis was performed
746 using ImageJ and was calculated using the "Spots colocalization (ComDet)" plugin developed
747 by Eugene A. Katrukha (Utrecht University, Netherlands). Golgi-derived tubules were
748 quantified manually upon Z-projection (maximum intensity) performed using the ImageJ
749 software.

750 **FLIP microscopy**

751 Growth media of the HeLa cells seeded on Nunc Lab-Tek 8-wells 1.0 bottom glass chamber
752 slides was supplemented with 25 mM HEPES (pH 7.4) prior to experiment. FLIP experiment
753 was performed on a TCS STED CW system (Leica) in confocal mode using a 63x XNA
754 objective and HyD detectors. Using the Live Data Mode tool of Las AF software (Leica),
755 intermittent bleaching steps were combined with imaging of the whole cell during ~35 min.

756 When the FLIP experiments were performed on a GFP-containing protein, the series consisted
757 of the following steps: (1) Image 512x512 pixels and pixel size ~75 nm, 200 Hz acquisition
758 speed, 5% nominal power of an Argon Laser (488 nm). (2) Do 6x bleaching steps, keeping the
759 same parameters as in step 1, but with a 100% laser power on a manually selected region
760 encompassing the entire cell except the Golgi region. (3) Repeat step 1. (4) Pause for 40 s. (5)
761 Repeat step 1. (6) Repeat steps 2–5 for 35 times.

762 When the FLIP experiments were performed on a mRFP-containing protein, the series
763 consisted of the following steps: (1) Image 512x512 pixels and pixel size ~75 nm, 200 Hz
764 acquisition speed, 15% nominal power of a HeNe Laser (543 nm). (2) Do 5x bleaching steps,
765 keeping the same parameters as in step 1, but with a 100% laser power on a manually selected
766 region encompassing the entire cell except the Golgi region. (3) Repeat step 1. (4) Pause for 42
767 s. (5) Repeat step 1. (6) Repeat steps 2–5 for 35 times.

768 To measure Golgi export rate of the protein of interest, the mean intensity of the region left by
769 the photobleaching mask (Golgi-including region), $I(t)$, was measured over time and
770 normalized to the initial intensity, $I_0 = I(t = 0)$, using ImageJ and plotted using Prism 9.1.2
771 (GraphPad). Data was finally fitted to a one-phase decay curve fixing the "plateau" to 0, that is
772 $I(t)/I_0 = exp(-t/\tau)$, from where the half-life, $t_{1/2} = ln(2)\,\tau$, is extracted, and used to
773 compare the Golgi residence time among different proteins.

774 **STORM imaging and data analysis**

775 For STORM imaging, HeLa cells were cultured on 8-chambered glass bottom dishes
776 (Thermoscientific) at 37 °C with 5% CO_2. Plasmids containing the sequence of the gene of

interest were transfected and 24 hours after, cells were fixed with 4% paraformaldehyde in PBS at room temperature for 15 minutes. After fixation, cells were washed, permeabilized with 0.1% Triton X-100 (Fisher Scientific) (v/v) in PBS for 10 minutes, washed again, and blocked in 3% BSA (Sigma Aldrich) (w/v) in PBS for 60 minutes. Then, cells were labeled with primary antibodies, as detailed in the "Immunofluorescence microscopy" section. Donkey-anti-rabbit conjugated with AF405/AF647 (3:1) and donkey-anti-mouse conjugated with Cy3/AF647 (7:1) were used as secondary antibodies at 2 µg/mL final concentration.

STORM was performed in an imaging buffer containing 10 mM Cysteamine MEA (SigmaAldrich), 0.5 mg/mL glucose oxidase (Sigma Aldrich), 40 µg/ml catalase (Sigma-Aldrich), and 6.25% glucose (Sigma Aldrich) in PBS (Gómez-García et al., 2018). Two-colour images were acquired on a commercial microscope system (Nikon Eclipse Ti N-STORM system), from Nikon Instruments, equipped with a 100x oil objective with NA 1.49 using oblique illumination. The detector was an ANDOR technology EMCCD iXon 897 camera, with a 256x256 pixel ROI and a pixel size of 160 nm. Fluorophore excitation was done using an Agilent technologies laser box with laser lines 405 nm, 561 nm, and 647 nm. NIS software (Nikon) was used for acquiring the data. In a pre-acquisition step the sample was irradiated with the 647 nm laser at 70% (~107 mW) power to bring a large majority of the dyes into a dark (off) state. STORM acquisition was then performed sequentially using 20 ms frames by maintaining the 647 nm laser at a constant power and using low power activator (405 nm or 561 nm) excitation (gradually increasing during acquisition from 0.5% to 100%). The acquisitions were stopped after ~70,000 frames.

STORM image reconstruction was performed in Insight3 software (Huang et al., 2008). The generated images were also corrected for cross-talked from images obtained from samples only labelled with 1 pair of antibodies. For the image reconstruction, a list containing the localization data for each channel were obtained. The degree of colocalization between both lists of localization was measured within a Golgi- containing region of interest (ROI) using the Coloc-Tesseler software (Levet et al., 2019). First, the software partition the image area into regions per localization where any given point within that region will be closer to that localization than to any other (Voronoi tessellation). Then, a first-rank density value, obtained from the area of the neighbour Voronoi areas, is assigned for each localization. Subsequently, these first-rank densities are represented in a logarithmic scaled scatterplot for each channel, always keeping channel A in x-axis and channel B in y-axis. The values in the scatterplot for channel A (x^A, y^A) correspond to the first-rank density of a localization in channel A (x^A) against the first-rank density of the localization of channel B in whose Voronoi area the point in channel A landed (y^A). Vice versa for the scatterplot associated to channel B.
Finally, the Spearman's rank correlation coefficients are quantified as a measure of the trength

813 and direction of the ranked variables plotted in each scatterplot. The Spearman's rank
814 correlation coefficient is defined as $S^A = 1 - \frac{6\sum_i\left(r(x_i^A)-r(y_i^A)\right)^2}{n_A({n_A}^2-1)}$, and $S^B = 1 -$
815 $\frac{6\sum_i\left(r(x_i^B)-r(y_i^B)\right)^2}{n_B({n_B}^2-1)}$, where $r\left(x_i^A\right)$ and $r\left(x_i^B\right)$ are the ranks of the first-rank density for channel A
816 in the scatterplots A and B respectively; $r\left(y_i^A\right)$ and $r\left(y_i^B\right)$ are the ranks of the first-rank density
817 of the channel B for the scatterplots A and B respectively; and n_A and n_B are the average
818 number of neighbours per channel. As the Pearson's correlation coefficient, the Spearman's
819 rank correlation coefficient varies from 1 (perfect localization) to -1 (perfect antilocalization)
820 and 0 representing a random distribution of localizations.

821 **Immunoprecipitation**

822 HeLa cells were lysed with lysis buffer (0.5% Triton X-100 in PBS) containing protease
823 inhibitors (Roche) for 15 min on ice, after which the samples were centrifuged at 16.000×g for
824 10 min at 4ºC. The resulting supernatants were incubated for 16 h while rotating at 4ºC with 8
825 µg/ml anti-GFP antibody (Roche). Protein A/G PLUS-Agarose (Santa Cruz) was then added to
826 the samples and incubated with rotation for 2 h at 4ºC. Immunoprecipitated fractions were
827 washed two times with lysis buffer and two more times with PBS, and heated to 95ºC for 5 min
828 with 1x Laemmli SDS sample buffer. The samples were subjected to SDS-PAGE and Western
829 blotting with anti-GFP (Santa Cruz) and anti-RFP (Abcam) antibodies.

830 **Secretion assay**

831 The growth media of HeLa WT and HeLa TGN46 KO cells seeded on a well of 6-wells plate -
832 and transfected with PAUF-Myc-His 48 h previous to the experiment performance- was
833 exchanged by pre-warmed (37ºC) DMEM containing 1% penicillin/streptomycin and 2 mM L-
834 Glutamine. Cells were then incubated for 4 h in an incubator at 37ºC and 5% CO_2 to collect
835 secreted PAUF-Myc-His protein. Then, media was collected in a 1.5 mL tube and centrifuged
836 to avoid floating dead cells that may interfere. Protease inhibitor was added to sample and
837 sample was concentrated down to 150 µL using Amicon Ultra-0.5 10 kDa Centrifugal Filter
838 Units (Merck). On the other hand, cells were lydes on ice with 150 uL of ice-cold lysis buffer
839 (1% SDS Tris-HCl pH 7.4). Samples were collected in a 1.5 mL tube using a scraper and
840 centrifuged at maximum speed for 20 min at 4ºC to remove cell pellet. Finally, 6x Laemmli
841 SDS sample buffer was added to both, supernatant and cell samples, and incubated for 10 min
842 at 95ºC. The samples were subjected to SDS-PAGE and Western blotting with anti-Myc (X)
843 and anti-TGN46 (AbD Serotec) antibodies. When cells were treated with BFA, the compound
844 was added to the cells to a final concentration of 5 µg/mL 15 min before media was exchanged
845 by FBS-deprived media and also to the collection media for the 4 h incubation time of the
846 secretion experiment.

847 **Protein production**

848 E. coli BL21 (DE3) cells transformed with pETM14-6his-mGFP -TGN46lum were grown at
849 37 °C to a density of OD600 0.6 in 2xYT medium containing Kanamycin (50 mg/l) with
850 shaking. Isopropyl-β-D-thiogalactoside (IPTG) was added to induce protein expression at a
851 final concentration of 0.2 mM, and the temperature was lowered to 18 °C. Cells were harvested
852 after 16 h by centrifugation and resuspended in TRIS buffer supplemented with 300 mM NaCl,
853 protease inhibitors (Roche), and lysed by French press cell disruptor. Lysate was clarified by
854 centrifugation. The supernatant was loaded onto HisTrap HP 5 ml columns (Cytiva), washed
855 and eluted by a linear gradient of 0–500 mM imidazole. The fractions containing the POI were
856 pooled, concentrated using Amicon Ultra-15 30 kDa MWCO centrifugal filter unit (EMD
857 Millipore), diluted in a TRIS buffer with 50ml NaCl and loaded onto a Hitrap Q 5ml column
858 (Cytiva) washed and eluted by a linear gradient of 50–700 mM NaCl. The fractions containing
859 the protein were collected, dialyzed again the storage buffer (20 mM TRIS pH7.4, 100 mM
860 NaCl and 10% glycerol), concentrated, and stored at −80 °C after flash freezing by liquid
861 nitrogen.

862 ***In vitro* characterization of biomolecular condensate formation**

863 The protein samples were dialyzed against 20 mM Tris-HCl and 1 mM TCEP at pH 7.5 and
864 concentrated to approximately 150 µM. All samples were prepared on ice as follows. First, a
865 buffer stock solution consisting of 20 mM Tris-HCl and 1mM TCEP was pH adjusted to 7.5
866 and filtered using 0.22 µm sterile filters (Buffer Stock). A 5 M NaCl solution in the same buffer
867 was also pH adjusted to 7.5 and filtered (Salt Stock). Then, the protein samples were centrifuged
868 for 5 minutes at 15,000 rpm at 5 ºC. The supernatant (Protein Stock) was transferred to a new
869 Eppendorf tube and the protein concentration was determined by its absorbance at 280 nm. A
870 64% (w/v) Ficoll 70 in water solution was prepared (Ficoll Stock). The final samples were
871 prepared by mixing the right amounts of Buffer Stock, Protein Stock, Salt Stock and Ficoll
872 Stock to reach the desired final protein, NaCl and Ficoll concentrations.

873 For microscopy experiments, 1.5 µl of sample was deposited in a sealed chamber comprising a
874 slide and a coverslip sandwiching double sided tape (3M 300 LSE high-temperature double-
875 sided tape of 0.17 mm thickness). The used coverslips were previously coated with PEG-silane
876 following the published protocol in Alberti et al (Alberti et al., 2018). Fluorescence microscopy
877 images and FRAP experiments were recorded using a Zeiss LSM780 confocal microscope
878 system with a Plan ApoChromat 63x 1.4 oil objective. For the FRAP experiment within a single
879 droplet, 20 droplets of similar size were selected and the bleached region was 30% of their
880 diameter. The intensity values were monitored for ROI1 (bleached area), ROI2 (entire droplet)
881 and ROI3 (background signal), and the data was fitted using the EasyFrap software

882 (Rapsomaniki et al., 2012) to extract the kinetic parameters.

883 For the turbidity assay, the absorbance of the samples was measured at 350 nm at the indicated
884 temperatures using 1 cm pathlength cuvettes and a Cary100 ultraviolet–visible
885 spectrophotometer equipped with a multicell thermoelectric temperature controller.

886 **Statistics**

887 Statistical significance was tested using One-Way ANOVA using GraphPad Prism 9.1.2, unless
888 otherwise stated in the figure legend. Different data sets were considered to be statistically
889 significant when the p-value was <0.05 (*); p-value<0.01 (**); p-value<0.001 (***); p-
890 value<0.0001 (****).

891 **REFERENCES**

892 Alberti, S., S. Saha, J.B. Woodruff, T.M. Franzmann, J. Wang, and A.A. Hyman. 2018. A
893 User's Guide for Phase Separation Assays with Purified Proteins. *J. Mol. Biol.*
894 430:4806–4820. doi:10.1016/j.jmb.2018.06.038.

895 Banani, S.F., H.O. Lee, A.A. Hyman, and M.K. Rosen. 2017. Biomolecular condensates:
896 Organizers of cellular biochemistry. *Nat. Rev. Mol. Cell Biol.* 18:285–298.
897 doi:10.1038/nrm.2017.7.

898 Banfield, D.K. 2011. Mechanisms of protein retention in the Golgi. *Cold Spring Harb.*
899 *Perspect. Biol.* 3:1–14. doi:10.1101/cshperspect.a005264.

900 Banting, G., R. Maile, and E.P. Roquemore. 1998. The steady state distribution of
901 humTGN46 is not significantly altered in cells defective in clathrin-mediated
902 endocytosis. *J. Cell Sci.* 111:3451–3458. doi:10.1242/jcs.111.23.3451.

903 Banting, G., and S. Ponnambalam. 1997. TGN38 and its orthologues: Roles in post-TGN
904 vesicle formation and maintenance of TGN morphology. *Biochim. Biophys. Acta - Mol.*
905 *Cell Res.* 1355:209–217. doi:10.1016/S0167-4889(96)00146-2.

906 von Blume, J., A.M. Alleaume, G. Cantero-Recasens, A. Curwin, A. Carreras-Sureda, T.
907 Zimmermann, J. van Galen, Y. Wakana, M.A. Valverde, and V. Malhotra. 2011.
908 ADF/cofilin regulates secretory cargo sorting at the TGN via the Ca2+ ATPase SPCA1.
909 *Dev. Cell*. 20:652–662. doi:10.1016/j.devcel.2011.03.014.

910 von Blume, J., A.M. Alleaume, C. Kienzle, A. Carreras-Sureda, M. Valverde, and V.
911 Malhotra. 2012. Cab45 is required for Ca2+;-dependent secretory cargo sorting at the
912 trans-Golgi network. *J. Cell Biol.* 199:1057–1066. doi:10.1083/jcb.201207180.

913 von Blume, J., J.M. Duran, E. Forlanelli, A.M. Alleaume, M. Egorov, R. Polishchuk, H.
914 Molina, and V. Malhotra. 2009. Actin remodeling by ADF/cofilin is required for cargo
915 sorting at the trans-Golgi network. *J. Cell Biol.* 187:1055–1069.
916 doi:10.1083/jcb.200908040.

917 von Blume, J., and A. Hausser. 2019. Lipid-dependent coupling of secretory cargo sorting
918 and trafficking at the trans-Golgi network. *FEBS Lett.* 593:2412–2427.
919 doi:10.1002/1873-3468.13552.

920 Boncompain, G., and A. V. Weigel. 2018. Transport and sorting in the Golgi complex:
921 multiple mechanisms sort diverse cargo. *Curr. Opin. Cell Biol.* 50:94–101.
922 doi:10.1016/j.ceb.2018.03.002.

923 Borgman, K.J.E., G. Flórez-Grau, M.A. Ricci, C. Manzo, M. Lakadamyali, A. Cambi, D.
924 Benítez-Ribas, F. Campelo, and M.F. Garcia-Parajo. 2020. Membrane receptor MerTK
925 is a newly identified transcriptional regulator that associates to chromatin as
926 nanoclusters during human DC differentiation. *bioRxiv*. 2020.04.16.044974.
927 doi:10.1101/2020.04.16.044974.

928 Bos, K., C. Wraight, and K.K. Stanley. 1993. TGN38 is maintained in the trans-Golgi
929 network by a tyrosine-containing motif in the cytoplasmic domain. *EMBO J.* 12:2219–
930 2228. doi:10.1002/j.1460-2075.1993.tb05870.x.

931 Bossard, C., D. Bresson, R.S. Polishchuk, and V. Malhotra. 2007. Dimeric PKD regulates
932 membrane fission to form transport carriers at the TGN. *J. Cell Biol.* 179:1123–1131.
933 doi:10.1083/jcb.200703166.

934 Brangwynne, C.P., C.R. Eckmann, D.S. Courson, A. Rybarska, C. Hoege, J. Gharakhani, F.
935 Jülicher, and A.A. Hyman. 2009. Germline P granules are liquid droplets that localize
936 by controlled dissolution/condensation. *Science (80-.).* 324:1729–1732.
937 doi:10.1126/science.1172046.

938 Braulke, T., and J.S. Bonifacino. 2009. Sorting of lysosomal proteins. *Biochim. Biophys. Acta*
939 *- Mol. Cell Res.* 1793:605–614. doi:10.1016/j.bbamcr.2008.10.016.

940 Bretscher, M.S., and S. Munro. 1993. Cholesterol and the golgi apparatus. *Science (80-.).*
941 261:1280–1281. doi:10.1126/science.8362242.

942 Campelo, F., J. van Galen, G. Turacchio, S. Parashuraman, M.M. Kozlov, M.F. García-
943 Parajo, and V. Malhotra. 2017. Sphingomyelin metabolism controls the shape and
944 function of the golgi cisternae. *Elife*. 6. doi:10.7554/eLife.24603.

945 Cancino, J., J.E. Jung, and A. Luini. 2013. Regulation of Golgi signaling and trafficking by
946 the KDEL receptor. *Histochem. Cell Biol.* 140:395–405. doi:10.1007/s00418-013-1130-
947 9.

948 Capasso, S., L. Sticco, R. Rizzo, M. Pirozzi, D. Russo, N.A. Dathan, F. Campelo, J. Galen,
949 M. Hölttä-Vuori, G. Turacchio, A. Hausser, V. Malhotra, I. Riezman, H. Riezman, E.
950 Ikonen, C. Luberto, S. Parashuraman, A. Luini, and G. D'Angelo. 2017. Sphingolipid
951 metabolic flow controls phosphoinositide turnover at the trans -Golgi network . *EMBO*
952 *J.* 36:1736–1754. doi:10.15252/embj.201696048.

953 Case, L.B., J.A. Ditlev, and M.K. Rosen. 2019. Regulation of Transmembrane Signaling by
954 Phase Separation. *Annu. Rev. Biophys.* 48:465–494. doi:10.1146/annurev-biophys-
955 052118-115534.

Castello-Serrano, I., F.A. Heberle, B. Diaz-Rohrer, R. Ippolito, C.R. Shurer, P. Lujan, F. Campelo, K.R. Levental, and I. Levental. 2023. Partitioning to ordered membrane domains regulates the kinetics of secretory traffic. *bioRxiv*. 2023.04.18.537395. doi:10.1101/2023.04.18.537395.

Cosson, P., J. Perrin, and J.S. Bonifacino. 2013. Anchors aweigh: Protein localization and transport mediated by transmembrane domains. *Trends Cell Biol.* 23:511–517. doi:10.1016/j.tcb.2013.05.005.

Crevenna, A.H., B. Blank, A. Maiser, D. Emin, J. Prescher, G. Beck, C. Kienzle, K. Bartnik, B. Habermann, M. Pakde, H. Leonhardt, D.C. Lamb, and J. von Blume. 2016. Secretory cargo sorting by Ca2+-dependent Cab45 oligomerization at the trans-Golgi network. *J. Cell Biol.* 213:305–314. doi:10.1083/jcb.201601089.

Curwin, A.J., J. von Blume, and V. Malhotra. 2012. Cofilin-mediated sorting and export of specific cargo from the Golgi apparatus in yeast. *Mol. Biol. Cell*. 23:2327–2338. doi:10.1091/mbc.E11-09-0826.

Deng, Y., M. Pakdel, B. Blank, E.L. Sundberg, C.G. Burd, and J. von Blume. 2018. Activity of the SPCA1 Calcium Pump Couples Sphingomyelin Synthesis to Sorting of Secretory Proteins in the Trans-Golgi Network. *Dev. Cell*. 47:464-478.e8. doi:10.1016/j.devcel.2018.10.012.

Deng, Y., F.E. Rivera-Molina, D.K. Toomre, and C.G. Burd. 2016. Sphingomyelin is sorted at the trans Golgi network into a distinct class of secretory vesicle. *Proc. Natl. Acad. Sci. U. S. A.* 113:6677–6682. doi:10.1073/pnas.1602875113.

Diaz-Rohrer, B.B., K.R. Levental, K. Simons, and I. Levental. 2014. Membrane raft association is a determinant of plasma membrane localization. *Proc. Natl. Acad. Sci. U. S. A.* 111:8500–8505. doi:10.1073/pnas.1404582111.

Dmitrieff, S., M. Rao, and P. Sens. 2013. Quantitative analysis of intra-Golgi transport shows intercisternal exchange for all cargo. *Proc. Natl. Acad. Sci. U. S. A.* 110:15692–15697. doi:10.1073/pnas.1303358110.

Dunn, K.W., M.M. Kamocka, and J.H. McDonald. 2011. A practical guide to evaluating colocalization in biological microscopy. *Am. J. Physiol. - Cell Physiol.* 300:C723. doi:10.1152/ajpcell.00462.2010.

Duran, J.M., F. Campelo, J. Van Galen, T. Sachsenheimer, J. Sot, M. V. Egorov, C. Rentero, C. Enrich, R.S. Polishchuk, F.M. Goñi, B. Brügger, F. Wieland, and V. Malhotra. 2012. Sphingomyelin organization is required for vesicle biogenesis at the Golgi complex.

989 *EMBO J.* 31:4535–4546. doi:10.1038/emboj.2012.317.

990 Ford, C., A. Parchure, J. von Blume, and C.G. Burd. 2021. Cargo sorting at the trans-Golgi
991 network at a glance. *J. Cell Sci.* 134. doi:10.1242/jcs.259110.

992 van Galen, J., F. Campelo, E. Martínez-Alonso, M. Scarpa, J.Á. Martínez-Menárguez, and V.
993 Malhotra. 2014. Sphingomyelin homeostasis is required to form functional enzymatic
994 domains at the trans-Golgi network. *J. Cell Biol.* 206:609–618.
995 doi:10.1083/jcb.201405009.

996 Garcia-Cabau, C., and X. Salvatella. 2021. Regulation of biomolecular condensate dynamics
997 by signaling. *Curr. Opin. Cell Biol.* 69:111–119. doi:10.1016/j.ceb.2021.01.002.

998 Gibson, D.G., L. Young, R.Y. Chuang, J.C. Venter, C.A. Hutchison 3rd, and H.O. Smith.
999 2009. Enzymatic assembly of DNA molecules up to several hundred kilobases. *Nat*
1000 *Methods*. 6:343–345. doi:10.1038/nmeth.1318.

1001 Gómez-García, P.A., E.T. Garbacik, J.J. Otterstrom, M.F. Garcia-Parajo, and M.
1002 Lakadamyali. 2018. Excitation-multiplexed multicolor superresolution imaging with fm-
1003 STORM and fm-DNA-PAINT. *Proc. Natl. Acad. Sci. U. S. A.* 115:12991–12996.
1004 doi:10.1073/pnas.1804725115.

1005 Guo, Y., D.W. Sirkis, and R. Schekman. 2014. Protein sorting at the trans-Golgi network.
1006 *Annu. Rev. Cell Dev. Biol.* 30:169–206. doi:10.1146/annurev-cellbio-100913-013012.

1007 Hirschberg, K., C.M. Miller, J. Ellenberg, J.F. Presley, E.D. Siggia, R.D. Phair, and J.
1008 Lippincott-Schwartz. 1998. Kinetic analysis of secretory protein traffic and
1009 characterization of Golgi to plasma membrane transport intermediates in living cells. *J.*
1010 *Cell Biol.* 143:1485–1503. doi:10.1083/jcb.143.6.1485.

1011 Huang, B., W. Wang, M. Bates, and X. Zhuang. 2008. Three-dimensional super-resolution
1012 imaging by stochastic optical reconstruction microscopy. *Science (80-.).* 319:810–813.
1013 doi:10.1126/science.1153529.

1014 Huet-Calderwood, C., F. Rivera-Molina, D. V. Iwamoto, E.B. Kromann, D. Toomre, and
1015 D.A. Calderwood. 2017. Novel ecto-tagged integrins reveal their trafficking in live cells.
1016 *Nat. Commun.* 8:1–13. doi:10.1038/s41467-017-00646-w.

1017 Humphrey, J.S., P.J. Peters, L.C. Yuan, and J.S. Bonifacino. 1993. Localization of TGN38 to
1018 the trans-Golgi network: Involvement of a cytoplasmic tyrosine-containing sequence. *J.*
1019 *Cell Biol.* 120:1123–1136. doi:10.1083/jcb.120.5.1123.

1020 Hyman, A.A., C.A. Weber, and F. Jülicher. 2014. Liquid-liquid phase separation in biology.

1021 *Annu. Rev. Cell Dev. Biol.* 30:39–58. doi:10.1146/annurev-cellbio-100913-013325.

1022 Jones, S.M., J.R. Crosby, J. Salamero, and K.E. Howell. 1993. A cytosolic complex of p62
1023 and rab6 associates with TGN38/41 and is involved in budding of exocytic vesicles
1024 from the trans-Golgi network. *J. Cell Biol.* 122:775–788. doi:10.1083/jcb.122.4.775.

1025 Kienzle, C., N. Basnet, A.H. Crevenna, G. Beck, B. Habermann, N. Mizuno, and J. von
1026 Blume. 2014. Cofilin recruits F-actin to SPCA1 and promotes Ca2+-mediated secretory
1027 cargo sorting. *J. Cell Biol.* 206:635–654. doi:10.1083/jcb.201311052.

1028 Kienzle, C., and J. von Blume. 2014. Secretory cargo sorting at the trans-Golgi network.
1029 *Trends Cell Biol.* 24:584–593. doi:10.1016/j.tcb.2014.04.007.

1030 Kulak, N.A., G. Pichler, I. Paron, N. Nagaraj, and M. Mann. 2014. Minimal, encapsulated
1031 proteomic-sample processing applied to copy-number estimation in eukaryotic cells.
1032 *Nat. Methods*. 11:319–324. doi:10.1038/nmeth.2834.

1033 Lee, S.S., and G. Banting. 2002. Characterisation of the lumenal domain of TGN38 and
1034 effects of elevated expression of TGN38 on glycoprotein secretion. *Eur. J. Cell Biol.*
1035 81:609–621. doi:10.1078/0171-9335-00279.

1036 Levet, F., G. Julien, R. Galland, C. Butler, A. Beghin, A. Chazeau, P. Hoess, J. Ries, G.
1037 Giannone, and J.B. Sibarita. 2019. A tessellation-based colocalization analysis approach
1038 for single-molecule localization microscopy. *Nat. Commun.* 10:1–12.
1039 doi:10.1038/s41467-019-10007-4.

1040 Li, Romero, Rani, Dunker, and Obradovic. 1999. Predicting Protein Disorder for N-, C-, and
1041 Internal Regions. *Genome Inform. Ser. Workshop Genome Inform.* 10:30–40.

1042 Liljedahl, M., Y. Maeda, A. Colanzi, I. Ayala, J. Van Lint, and V. Malhotra. 2001. Protein
1043 Kinase D regulates the fission of cell surface destined transport carriers from the trans-
1044 Golgi network. *Cell*. 104:409–420. doi:10.1016/S0092-8674(01)00228-8.

1045 Lippincott-Schwartz, J., and R.D. Phair. 2010. Lipids and cholesterol as regulators of traffic
1046 in the endomembrane system. *Annu. Rev. Biophys.* 39:559–578.
1047 doi:10.1146/annurev.biophys.093008.131357.

1048 Lorent, J.H., B. Diaz-Rohrer, X. Lin, K. Spring, A.A. Gorfe, K.R. Levental, and I. Levental.
1049 2017. Structural determinants and functional consequences of protein affinity for
1050 membrane rafts. *Nat. Commun.* 8. doi:10.1038/s41467-017-01328-3.

1051 Luini, A., and S. Parashuraman. 2016. Signaling at the Golgi: Sensing and controlling the
1052 membrane fluxes. *Curr. Opin. Cell Biol.* 39:37–42. doi:10.1016/j.ceb.2016.01.014.

1053 Lujan, P., J. Angulo-Capel, M. Chabanon, and F. Campelo. 2021. Interorganelle
1054 communication and membrane shaping in the early secretory pathway. *Curr. Opin. Cell*
1055 *Biol.* 71:95–102. doi:10.1016/j.ceb.2021.01.010.

1056 Lujan, P., and F. Campelo. 2021. Should I stay or should I go? Golgi membrane spatial
1057 organization for protein sorting and retention. *Arch. Biochem. Biophys.* 707:108921.
1058 doi:10.1016/j.abb.2021.108921.

1059 Luzio, J.P., B. Brake, G. Banting, K.E. Howell, P. Braghetta, and K.K. Stanley. 1990.
1060 Identification, sequencing and expression of an integral membrane protein of the trans-
1061 Golgi network (TGN38). *Biochem. J.* 270:97–102. doi:10.1042/bj2700097.

1062 Malhotra, V., and F. Campelo. 2011. PKD regulates membrane fission to generate TGN to
1063 cell surface transport carriers. *Cold Spring Harb. Perspect. Biol.* 3:1–9.
1064 doi:10.1101/cshperspect.a005280.

1065 Mallet, W.G., and F.R. Maxfield. 1999. Chimeric forms of furin and TGN38 are transported
1066 from the plasma membrane to the trans-Golgi network via distinct endosomal pathways.
1067 *J. Cell Biol.* 146:345–359. doi:10.1083/jcb.146.2.345.

1068 Di Martino, R., L. Sticco, and A. Luini. 2019. Regulation of cargo export and sorting at the
1069 trans-Golgi network. *FEBS Lett.* 593:2306–2318. doi:10.1002/1873-3468.13572.

1070 McNamara, J.O., J.C. Grigston, H.M.A. VanDongen, and A.M.J. VanDongen. 2004. Rapid
1071 dendritic transport of TGN38, a putative cargo receptor. *Mol. Brain Res.* 127:68–78.
1072 doi:10.1016/j.molbrainres.2004.05.013.

1073 Van Meer, G., D.R. Voelker, and G.W. Feigenson. 2008. Membrane lipids: Where they are
1074 and how they behave. *Nat. Rev. Mol. Cell Biol.* 9:112–124. doi:10.1038/nrm2330.

1075 Milovanovic, D., A. Honigmann, S. Koike, F. Göttfert, G. Pähler, M. Junius, S. Müllar, U.
1076 DIederichsen, A. Janshoff, H. Grubmüller, H.J. Risselada, C. Eggeling, S.W. Hell, G.
1077 Van Den Bogaart, and R. Jahn. 2015. Hydrophobic mismatch sorts SNARE proteins
1078 into distinct membrane domains. *Nat. Commun.* 6:5984. doi:10.1038/ncomms6984.

1079 Mitra, K., I. Ubarretxena-Belandia, T. Taguchi, G. Warren, and D.M. Engelman. 2004.
1080 Modulation of the bilayer thickness of exocytic pathway membranes by membrane
1081 proteins rather than cholesterol. *Proc. Natl. Acad. Sci. U. S. A.* 101:4083–4088.
1082 doi:10.1073/pnas.0307332101.

1083 Mittag, T., and R. V. Pappu. 2022. A conceptual framework for understanding phase
1084 separation and addressing open questions and challenges. *Mol. Cell*. 82:2201–2214.

1085 doi:10.1016/J.MOLCEL.2022.05.018.

1086 Munro, S. 1991. Sequences within and adjacent to the transmembrane segment of α-2, 6-
1087 sialyltransferase specify Golgi retention. *EMBO J.* 10:3577–3588. doi:10.1002/j.1460-
1088 2075.1991.tb04924.x.

1089 Munro, S. 1995. An investigation of the role of transmembrane domains in Golgi protein
1090 retention. *EMBO J.* 14:4695–4704. doi:10.1002/j.1460-2075.1995.tb00151.x.

1091 Ohno, H., M.C. Fournier, G. Poy, and J.S. Bonifacino. 1996. Structural determinants of
1092 interaction of tyrosine-based sorting signals with the adaptor medium chains. *J. Biol.*
1093 *Chem.* 271:29009–29015. doi:10.1074/jbc.271.46.29009.

1094 Parchure, A., M. Tian, D. Stalder, C.K. Boyer, S.C. Bearrows, K.E. Rohli, J. Zhang, F.
1095 Rivera-Molina, B.R. Ramazanov, S.K. Mahata, Y. Wang, S.B. Stephens, D.C.
1096 Gershlick, and J. von Blume. 2022. Liquid–liquid phase separation facilitates the
1097 biogenesis of secretory storage granules. *J. Cell Biol.* 221. doi:10.1083/jcb.202206132.

1098 Patterson, G.H., K. Hirschberg, R.S. Polishchuk, D. Gerlich, R.D. Phair, and J. Lippincott-
1099 Schwartz. 2008. Transport through the Golgi Apparatus by Rapid Partitioning within a
1100 Two-Phase Membrane System. *Cell*. 133:1055–1067. doi:10.1016/j.cell.2008.04.044.

1101 Pecot, M.Y., and V. Malhotra. 2004. Golgi membranes remain segregated from the
1102 endoplasmic reticulum during mitosis in mammalian cells. *Cell*. 116:99–107.

1103 Ponnambalam, S., M. Girotti, M.L. Yaspo, C.E. Owen, A.C.F. Perry, T. Suganuma, T.
1104 Nilsson, M. Fried, G. Banting, and G. Warren. 1996. Primate homologues of rat
1105 TGN38: Primary structure, expression and functional implications. *J. Cell Sci.* 109:675–
1106 685. doi:10.1242/jcs.109.3.675.

1107 Quiroga, R., A. Trenchi, A.G. Montoro, J.V. Taubas, and H.J.F. Maccioni. 2013. Short
1108 transmembrane domains with high-volume exoplasmic halves determine retention of
1109 type II membrane proteins in the golgi complex. *J. Cell Sci.* 126:5344–5349.
1110 doi:10.1242/jcs.130658.

1111 Rajasekaran, A.K., J.S. Humphrey, M. Wagner, G. Miesenböck, A. Le Bivic, J.S. Bonifacino,
1112 and E. Rodriguez-Boulan. 1994. TGN38 recycles basolaterally in polarized Madin-
1113 Darby canine kidney cells. *Mol. Biol. Cell*. 5:1093–1103. doi:10.1091/mbc.5.10.1093.

1114 Ramazanov, B.R., M.L. Tran, and J. von Blume. 2021. Sending out molecules from the TGN.
1115 *Curr. Opin. Cell Biol.* 71:55–62. doi:10.1016/j.ceb.2021.02.005.

1116 Rapsomaniki, M.A., P. Kotsantis, I.E. Symeonidou, N.N. Giakoumakis, S. Taraviras, and Z.

1117 Lygerou. 2012. EasyFRAP: An interactive, easy-to-use tool for qualitative and
1118 quantitative analysis of FRAP data. *Bioinformatics*. 28:1800–1801.
1119 doi:10.1093/bioinformatics/bts241.

1120 Reaves, B., M. Horn, and G. Banting. 1993. TGN38/41 recycles between the cell surface and
1121 the TGN: Brefeldin A affects its rate of return to the TGN. *Mol. Biol. Cell*. 4:93–105.
1122 doi:10.1091/mbc.4.1.93.

1123 Romero, Obradovic, and Dunker. 1997. Sequence Data Analysis for Long Disordered
1124 Regions Prediction in the Calcineurin Family. *Genome Inform. Ser. Workshop Genome*
1125 *Inform.* 8:110–124.

1126 Sharpe, H.J., T.J. Stevens, and S. Munro. 2010. A Comprehensive Comparison of
1127 Transmembrane Domains Reveals Organelle-Specific Properties. *Cell*. 142:158–169.
1128 doi:10.1016/j.cell.2010.05.037.

1129 Shin, Y., and C.P. Brangwynne. 2017. Liquid phase condensation in cell physiology and
1130 disease. *Science (80-.).* 357. doi:10.1126/science.aaf4382.

1131 Sickmeier, M., J.A. Hamilton, T. LeGall, V. Vacic, M.S. Cortese, A. Tantos, B. Szabo, P.
1132 Tompa, J. Chen, V.N. Uversky, Z. Obradovic, and A.K. Dunker. 2007. DisProt: The
1133 database of disordered proteins. *Nucleic Acids Res.* 35. doi:10.1093/nar/gkl893.

1134 Spang, A. 2015. The road not taken: Less traveled roads from the TGN to the plasma
1135 membrane. *Membranes (Basel).* 5:84–98. doi:10.3390/membranes5010084.

1136 Stalder, D., and D.C. Gershlick. 2020. Direct trafficking pathways from the Golgi apparatus
1137 to the plasma membrane. *Semin. Cell Dev. Biol.* 107:112–125.
1138 doi:10.1016/j.semcdb.2020.04.001.

1139 Stanley, K.K., and K.E. Howell. 1993. TGN38/41: a molecule on the move. *Trends Cell Biol.*
1140 3:252–255. doi:10.1016/0962-8924(93)90046-4.

1141 Tie, H.C., D. Mahajan, and L. Lu. 2022. Visualizing intra-Golgi localization and transport by
1142 side-averaging Golgi ministacks. *J. Cell Biol.* 221. doi:10.1083/jcb.202109114.

1143 Tu, L., W.C.S. Tai, L. Chen, and D.K. Banfield. 2008. Signal-mediated dynamic retention of
1144 glycosyltransferases in the Golgi. *Science (80-.).* 321:404–407.
1145 doi:10.1126/science.1159411.

1146 Vacic, V., V.N. Uversky, A.K. Dunker, and S. Lonardi. 2007. Composition Profiler: A tool
1147 for discovery and visualization of amino acid composition differences. *BMC*
1148 *Bioinformatics*. 8. doi:10.1186/1471-2105-8-211.

1149 Wakana, Y., and F. Campelo. 2021. The PKD-dependent biogenesis of TGN-to-plasma
1150 membrane transport carriers. *Cells*. 10:1618. doi:10.3390/cells10071618.

1151 Wakana, Y., J. Van Galen, F. Meissner, M. Scarpa, R.S. Polishchuk, M. Mann, and V.
1152 Malhotra. 2012. A new class of carriers that transport selective cargo from the trans
1153 Golgi network to the cell surface. *EMBO J.* 31:3976–3990.
1154 doi:10.1038/emboj.2012.235.

1155 Wakana, Y., K. Hayashi, T. Nemoto, C. Watanabe, M. Taoka, J. Angulo-Capel, M.F. Garcia-
1156 Parajo, H. Kumata, T. Umemura, H. Inoue, K. Arasaki, F. Campelo, and M. Tagaya.
1157 2021. The ER cholesterol sensor SCAP promotes CARTS biogenesis at ER–golgi
1158 membrane contact sites. *J. Cell Biol.* 220. doi:10.1083/jcb.202002150.

1159 Wakana, Y., R. Kotake, N. Oyama, M. Murate, T. Kobayashi, K. Arasaki, H. Inoue, and M.
1160 Tagaya. 2015. CARTS biogenesis requires VAP-lipid transfer protein complexes
1161 functioning at the endoplasmic reticulum-Golgi interface. *Mol. Biol. Cell*. 26:4686–
1162 4699. doi:10.1091/mbc.E15-08-0599.

1163 Wakana, Y., J. Villeneuve, J. van Galen, D. Cruz-Garcia, M. Tagaya, and V. Malhotra. 2013.
1164 Kinesin-5/Eg5 is important for transport of CARTS from the trans-Golgi network to the
1165 cell surface. *J. Cell Biol.* 202:241–250. doi:10.1083/jcb.201303163.

1166 Wang, J., and K.E. Howell. 2000. The luminal domain of TGN38 interacts with integrin β1
1167 and is involved in its trafficking. *Traffic*. 1:713–723. doi:10.1034/j.1600-
1168 0854.2000.010904.x.

1169 Wang, J., M.S. Ladinsky, and K.E. Howell. 1995. Molecules and vesicle coats involved in the
1170 budding of exocytotic vesicles from the trans-Golgi network. *Cold Spring Harb. Symp.*
1171 *Quant. Biol.* 60:139–146. doi:10.1101/SQB.1995.060.01.017.

1172 Welch, L.G., and S. Munro. 2019. A tale of short tails, through thick and thin: investigating
1173 the sorting mechanisms of Golgi enzymes. *FEBS Lett.* 593:2452–2465.
1174 doi:10.1002/1873-3468.13553.

1175 Welch, L.G., S.Y. Peak-Chew, F. Begum, T.J. Stevens, and S. Munro. 2021. Golph3 and
1176 golph3l are broad-spectrum copi adaptors for sorting into intra-golgi transport vesicles.
1177 *J. Cell Biol.* 220. doi:10.1083/jcb.202106115.

1178 Wood, C.S., K.R. Schmitz, N.J. Bessman, T.G. Setty, K.M. Ferguson, and C.G. Burd. 2009.
1179 PtdIns4P recognition by Vps74/GOLPH3 links PtdIns 4-kinase signaling to retrograde
1180 Golgi trafficking. *J. Cell Biol.* 187:967–975. doi:10.1083/jcb.200909063.

1181 Yeaman, C., M.I. Ayala, J.R. Wright, F. Bard, C. Bossard, A. Ang, Y. Maeda, T. Seufferlein,
1182 I. Mellman, W.J. Nelson, and V. Malhotra. 2004. Protein kinase D regulates basolateral
1183 membrane protein exit from trans-Golgi network. *Nat. Cell Biol.* 6:106–112.
1184 doi:10.1038/ncb1090.

1185 Zappa, F., M. Failli, and M.A. De Matteis. 2018. The Golgi complex in disease and therapy.
1186 *Curr. Opin. Cell Biol.* 50:102–116. doi:10.1016/j.ceb.2018.03.005.

1187 Zhang, J., A. Kennedy, L. Xing, S. Bui, W. Reid, J. Joppich, E. Ahat, M. Rose, Q. Tang,
1188 A.W. Tai, and Y. Wang. 2022. SARS-CoV-2 triggers Golgi fragmentation via down-
1189 regulation of GRASP55 to facilitate viral trafficking. *bioRxiv Prepr. Serv. Biol.*
1190 2022.03.04.483074. doi:10.1101/2022.03.04.483074.

1191